ORIGINAL ARTICLE

Assessment of CMIP6 Performance and Projected Temperature and Precipitation Changes Over South America

Mansour Almazroui[1,2] · Moetasim Ashfaq[3] · M. Nazrul Islam[1] · Irfan Ur Rashid[4] · Shahzad Kamil[4] ·
Muhammad Adnan Abid[5] · Enda O'Brien[6] · Muhammad Ismail[1] · Michelle Simões Reboita[7] · Anna A. Sörensson[8,9,10] ·
Paola A. Arias[11] · Lincoln Muniz Alves[12] · Michael K. Tippett[13] · Sajjad Saeed[5,14] · Rein Haarsma[15] ·
Francisco J. Doblas-Reyes[16,17] · Fahad Saeed[18] · Fred Kucharski[5] · Imran Nadeem[19] · Yamina Silva-Vidal[20] ·
Juan A. Rivera[21,22] · Muhammad Azhar Ehsan[23] · Daniel Martínez-Castro[24] · Ángel G. Muñoz[23] · Md. Arfan Ali[25] ·
Erika Coppola[5] · Mouhamadou Bamba Sylla[26]

Abstract

We evaluate the performance of a large ensemble of Global Climate Models (GCMs) from the Coupled Model Intercomparison Project Phase 6 (CMIP6) over South America for a recent past reference period and examine their projections of twenty-first century precipitation and temperature changes. The future changes are computed for two time slices (2040–2059 and 2080–2099) relative to the reference period (1995–2014) under four Shared Socioeconomic Pathways (SSPs, SSP1–2.6, SSP2–4.5, SSP3–7.0 and SSP5–8.5). The CMIP6 GCMs successfully capture the main climate characteristics across South America. However, they exhibit varying skill in the spatiotemporal distribution of precipitation and temperature at the sub-regional scale, particularly over high latitudes and altitudes. Future precipitation exhibits a decrease over the east of the northern Andes in tropical South America and the southern Andes in Chile and Amazonia, and an increase over southeastern South America and the northern Andes—a result generally consistent with earlier CMIP (3 and 5) projections. However, most of these changes remain within the range of variability of the reference period. In contrast, temperature increases are robust in terms of magnitude even under the SSP1–2.6. Future changes mostly progress monotonically from the weakest to the strongest forcing scenario, and from the mid-century to late-century projection period. There is an increase in the seasonality of the intra-annual precipitation distribution, as the wetter part of the year contributes relatively more to the annual total. Furthermore, an increasingly heavy-tailed precipitation distribution and a rightward shifted temperature distribution provide strong indications of a more intense hydrological cycle as greenhouse gas emissions increase. The relative distance of an individual GCM from the ensemble mean does not substantially vary across different scenarios. We found no clear systematic linkage between model spread about the mean in the reference period and the magnitude of simulated sub-regional climate change in the future period. Overall, these results could be useful for regional climate change impact assessments across South America.

Keywords CMIP6 · Climate change · Global climate models · South America

1 Introduction

Like many other regions across the planet, South America has experienced environmental changes during the twentieth century, including increasing surface temperatures (Salviano et al. 2016; de Barros Soares et al. 2017; Dereczynski et al.

2020; Pabon-Caicedo et al. 2020), shifting precipitation patterns (Espinoza et al. 2019; Paca et al. 2020; Marrafon et al. 2020; Carvalho 2020; Giráldez et al. 2020; Pabon-Caicedo et al. 2020), vanishing Andean glaciers (Schauwecker et al. 2014; Malmros et al. 2016; Drenkhan et al. 2018; Vuille et al. 2018; Somers et al. 2019; Masiokas et al. 2020), and an increase in weather and climate extremes, such as droughts, floods, and wildfires (Barros et al. 2015; Martins et al. 2018; Viganó et al. 2018; Cunha et al. 2019; Feron et al. 2019; Lemes et al. 2020; Debortoli et al. 2020; Zubieta et al.

✉ Mansour Almazroui
mansour@kau.edu.sa

Extended author information available on the last page of the article

2021). Such variations in climate characteristics are precursors to what may lie ahead in the coming decades for this continent if the unprecedented rise in greenhouse gas emissions continues. The Amazon, which is the world's largest rainforest and comprises more than 35% of the continent, has a profound impact on the Earth's climate due to its role in the global energy, moisture, and carbon balances (Zhang et al. 2015; Phillips et al. 2017). Over the past several decades, it is feared that human-induced changes have contributed to reduced rainfall over parts of the Amazon, increasing the vulnerability of its ecosystem to droughts and wildfires (Brando et al. 2014, 2019; Boisier et al. 2015; Duffy et al. 2015; De Faria et al. 2017; Silva et al. 2018; Marengo et al. 2018; Barkhordarian et al. 2019; Cook et al. 2020; Parsons 2020) and threatening the delicate balance of the Earth System. The Andes are home to 99% of the world's remaining tropical glaciers (Yarleque et al. 2018; Rabatel et al. 2013; Veettil and Kamp 2019), which are retreating at a rate not seen in recorded history (López-Moreno et al. 2014; Schauwecker et al. 2014; Veettil and Kamp 2019; Masiokas et al. 2020). Changing climate patterns may also have a significant role in soil degradation and desertification—an issue faced by several countries across the continent (Spinoni et al. 2015; Pérez et al. 2017; Vieira et al. 2021)—which has serious consequences for social-ecological sustainability and food security.

The climate of South America varies widely from North to South and West to East, due to its large latitudinal extent and topographic heterogeneity (Garreaud et al. 2009; Reboita et al. 2010; Espinoza et al. 2020; Arias et al. 2021a). The northern and central parts of South America have a tropical climate; arid desert and steppe climate characterizes the western edge, the southeast is relatively temperate, while the southwestern edge has a polar tundra climate (Beck et al. 2018). The variety of climate characteristics across South America is evident from the fact that the equatorial region in Colombia is one of the wettest areas on the planet (Poveda and Mesa 2000; Espinoza et al. 2020; Mejía et al. 2021) while the western Atacama Desert in Chile is the driest place on Earth (Ritter et al. 2019; Schween et al. 2020). Following the Atacama Desert, the semiarid Northeast of Brazil is the second driest region in South America (Reboita et al. 2016). Precipitation has strong spatial–temporal variability with marked seasonal variability over the monsoon region (Marengo et al. 2012; Espinoza et al. 2020; Grimm et al. 2020) and relatively less seasonal variability over the southern and western parts with the exception of the western slopes of the extratropical Andes in Chile (Schumacher et al. 2020; Grimm et al. 2020). Realistic representation of the complex climate characteristics of South America in numerical models remains a challenge. For instance, most studies using Global Climate Models (GCMs) show that while models are able to simulate the main precipitation,

temperature and circulation features over the continent, they exhibit systematic errors in precipitation magnitudes, such as underestimation in tropical South America and overestimation in the Andes and La Plata basin (Yin et al. 2013; Gulizia and Camilloni 2015; Sierra et al. 2015; Zazulie et al. 2017; Rivera and Arnould 2020; Arias et al. 2021b; Dias and Reboita 2021; Ortega et al. 2021). Several studies also document the limitations of GCMs in simulating mesoscale circulation features associated with the Andes (Pabón-Caicedo et al. 2020; Arias et al. 2021a), and the genesis of mesoscale convective systems over southeastern South America (Muñoz et al. 2015, 2016; Doss-Gollin 2018).

Every new iteration of the Coupled Model Intercomparison Project (CMIP) is based on the premise that newer generations of GCMs will demonstrate improvements over the previous ones, as models progressively improve in terms of their computational efficiency, resolution and representation of physical processes. In the latest 6th phase of CMIP (CMIP6, O'Neill, 2016; Petrie et al. 2021), GCMs are forced with a new set of scenarios, which are a combination of Shared Socioeconomic Pathways (SSPs; Riahi et al. 2017) and Representative Concentration Pathways (RCPs; van Vuuren et al. 2011), to understand the Earth system response to increased anthropogenic forcing. The pathways addressed in this paper range from SSP1-2.6 representing one of the weaker forcing scenarios, to SSP5–8.5 representing the strongest forcing trajectory (O'Neill et al. 2016; Riahi et al. 2017; Zelinka et al. 2020). Given the availability of new sets of CMIP GCMs and future SSP-RCP scenarios, there is a need to establish new guidelines related to potential climate changes in the coming decades over South America. Several factors should be kept in mind in the evaluation of CMIP6 GCMs for future climate projections. First, as previously noted, a strong heterogeneity in climate characteristics exists throughout the continent, and precipitation seasonality also varies across the region (Reboita et al. 2010). Consequently, sub-regional GCM evaluation is necessary to fully understand the potential diversity of changes in future climate over different climate zones. Second, research on the implications of climate change for natural and human systems is rapidly increasing. To this end, GCM output, directly or after downscaling, is now commonly used for making climate change hazard and risk assessments. Since robust climate change information is required for informed decision making, the identification of median values and outliers in the CMIP6 ensemble—both in terms of historical biases and future climate change—is important for improving the reliability of climate risk assessments. Third, the range of potential future climatic changes depends not only on the choice of future scenarios, but also on the diversity of GCMs and projection time periods. Therefore, a comprehensive

understanding of climate change uncertainty over South America can only emerge if all factors affecting variations in time and space are fully explored. Recent studies highlight that CMIP6 models improve the representation of seasonal precipitation in South America with respect to CMIP3 and CMIP5 (Arias et al. 2021b; Dias and Reboita 2021; Ortega et al. 2021) although systematic large-scale biases such as the double Intertropical Convergence Zone still persist (Tian and Dong 2020; Ortega et al. 2021).

In this study, we analyze a large suite of CMIP6 GCMs over the historical and twenty-first century projection periods under four future climate scenarios. In addition to spatial analyses over the whole continent, South America is divided into seven sub-regions, following Iturbide et al. (2020), to account for its heterogeneity in climate characteristics. Over each sub-region, comparative analyses across scenarios, GCMs and two future time periods (mid-century and late-century) focus on the investigation of model biases, future climate sensitivity, and the distribution of simulated monthly total precipitation and temperature changes in space and time.

2 Data and Methodology

For the comparison of model simulations with observations during the historical period, we obtained observed monthly precipitation and temperature data from multiple sources (see Table 1 for details). The corresponding simulated data from 38 CMIP6 models were obtained from Earth System Grid Federation (ESGF) archives (https://esgf-node.llnl.gov/search/cmip6), for the historical period and four future scenarios, namely SSP1–2.6 (SSP126), SSP2–4.5 (SSP245), SSP3–7.0 (SSP370) and SSP5–8.5 (SSP585). Note that SSP370 analyses were based on the 35 available GCMs (see Table 2). We considered three time periods for our analyses, including 1995–2014 as reference climate, 2040–2059 as mid-century future, and 2080–2099 as late-century future. In addition to spatial analyses over the whole South American domain, we divided the continent into seven sub-regions (Fig. 1). All GCMs and observations were spatially remapped to a common 1° × 1° lat-lon grid with a bilinear interpolation.

As mentioned above, intra-annual precipitation characteristics vary substantially across South America, and therefore, there is no objective universal definition of wet and dry

Table 1 Details of the observational datasets used in this study

Variable	Full name	Method	Resolution (lat × lon)	Weblink
Precipitation	Climate Hazards group Infra-Red Precipitation with Stations (CHIRPS v2.0)	Satellite + guage	0.05° × 0.05°	https://www.chc.ucsb.edu/data/chirps
	Climatic Research Unit (CRU v4.04)	Digital Curation	0.5° × 0.5°	https://crudata.uea.ac.uk/cru/data/hrg/cru_ts_4.04
	Climate Prediction Center Merged Analysis of Precipitation (CMAP v2104)	Satellite + Guage	2.5° × 2.5°	https://psl.noaa.gov/data/gridded/data.cmap.html
	Global Precipitation Climatology Centre (GPCC v2018)	Guage	1.0° × 1.0°	https://psl.noaa.gov/data/gridded/data.gpcc.html
	Global Precipitation Climatology Project (GPCP v2.3)	Satellite + Guage	2.5° × 2.5°	https://psl.noaa.gov/data/gridded/data.gpcp.html
	Precipitation Estimation from Remotely Sensed Information using Artificial Neural Networks- Climate Data Record (PERSIANN-CDR v1)	Satellite + Artificial Intelligence	0.25° × 0.25°	https://climatedataguide.ucar.edu/climate-data/persiann-cdr-precipitation-estimation-remotely-sensed-information-using-artificial
	TerraClimate	Digital Curation	0.04° × 0.04°	http://www.climatologylab.org/terraclimate.html
	University of Delaware (UoD v5.01)		0.5° × 0.5°	https://psl.noaa.gov/data/gridded/data.UDel_AirT_Precip.html
Surface Air Temperature	Climatic Research Unit (CRU v4.04)	Digital Curation	0.5° × 0.5°	https://crudata.uea.ac.uk/cru/data/hrg/cru_ts_4.04
	TerraClimate	Digital Curation	0.04° × 0.04°	http://www.climatologylab.org/terraclimate.html
	University of Delaware (UoD v5.01)		0.5° × 0.5°	https://psl.noaa.gov/data/gridded/data.UDel_AirT_Precip.html

Table 2 Details of the 38 CMIP6 GCMs used in this study, along with their country of origin and resolutions

No.	CMIP6 model name	Country	Horizontal grid spacing (in degrees)	Variant label
1	ACCESS-CM2	Australia	1.9°×1.3°	r1i1p1f1
2	ACCESS-ESM1-5	Australia	1.9°×1.2°	r1i1p1f1
3	AWI-CM-1–1-MR	Germany	0.9°×0.9°	r1i1p1f1
4	BCC-CSM2-MR	China	1.1°×1.1°	r1i1p1f1
5	CAMS-CSM1-0	China	1.1°×1.1°	r1i1p1f1
6	CanESM5-CanOE	Canada	2.8°×2.8°	r1i1p2f1
7	CanESM5	Canada	2.8°×2.8°	r1i1p1f1
8	CESM2	USA	1.3°×0.9°	r4i1p1f1
9	CESM2-WACCM	USA	1.3°×0.9°	r1i1p1f1
10	CMCC-CM2-SR5	Italy	1.3°×0.9°	r1i1p1f1
11	CMCC-ESM2	Italy	1.3°×0.9°	r1i1p1f1
12	CNRM-CM6-1	France	1.4°×1.4°	r1i1p1f2
13	CNRM-CM6-1-HR	France	0.5°×0.5°	r1i1p1f2
14	CNRM-ESM2-1	France	1.4°×1.4°	r1i1p1f2
15	EC-Earth3	Europe	0.7°×0.7°	r1i1p1f1
16	EC-Earth3-Veg-LR	Europe	1.1°×1.1°	r1i1p1f1
17	EC-Earth3-Veg	Europe	0.7°×0.7°	r2i1p1f1
18	FGOALS-f3-L	China	1.3°×1°	r1i1p1f1
19	FGOALS-g3	China	2°×2.3°	r1i1p1f1
20	FIO-ESM-2-0*	China	1.3°×0.9°	r1i1p1f1
21	GFDL-ESM4	USA	1.3°×1°	r1i1p1f1
22	GISS-E2-1-G	USA	2.5°×2°	r1i1p1f2
23	HadGEM3-GC31-LL*	UK	1.9°×1.3°	r1i1p1f3
24	IITM-ESM	India	1.9°×1.9°	r1i1p1f1
25	INM-CM4-8	Russia	2°×1.5°	r1i1p1f1
26	INM-CM5-0	Russia	2°×1.5°	r1i1p1f1
27	IPSL-CM6A-LR	France	2.5°×1.3°	r1i1p1f1
28	MCM-UA-1-0	USA	3.8°×2.3°	r1i1p1f2
29	MIROC6	Japan	1.4°×1.4°	r1i1p1f1
30	MIROC-ES2L	Japan	2.8°×2.8°	r1i1p1f2
31	MPI-ESM1-2-HR	Germany	0.9°×0.9°	r1i1p1f1
32	MPI-ESM1-2-LR	Germany	1.9°×1.9°	r1i1p1f1
33	MRI-ESM2-0	Japan	1.1°×1.1°	r1i1p1f1
34	NESM3*	China	1.9°×1.9°	r1i1p1f1
35	NorESM2-LM	Norway	2.5°×1.9°	r1i1p1f1
36	NorESM2-MM	Norway	0.9°×1.3°	r1i1p1f1
37	TaiESM1	Taiwan	1.3°×1°	r1i1p1f1
38	UKESM1-0-LL	UK	1.9°×1.3°	r1i1p1f2

Note that the variant label provides information about realization (*r*), initialization method (*i*), physics (*p*), and forcing (*f*)

*These models are not available for SSP3–7.0

seasons that is suitable for the entire continent. However, several earlier studies used October to March as a wet season and April to September as a dry season (Reboita et al. 2014; Bellprat et al. 2015; Coelho et al. 2016; Nielsen et al. 2016). Therefore, in our spatial analyses, we evaluated GCMs at annual and these two 6-monthly time periods. We also analyzed precipitation (temperature) amplitudes at each grid point, which are defined as the difference between the wettest (hottest) and driest (coldest) months at climatological scale. In addition, we performed domain-averaged annual cycle analyses for precipitation over each sub-region.

The spatiotemporal distributions of monthly precipitation and temperature in the reference period and their corresponding changes in the future periods were further analyzed
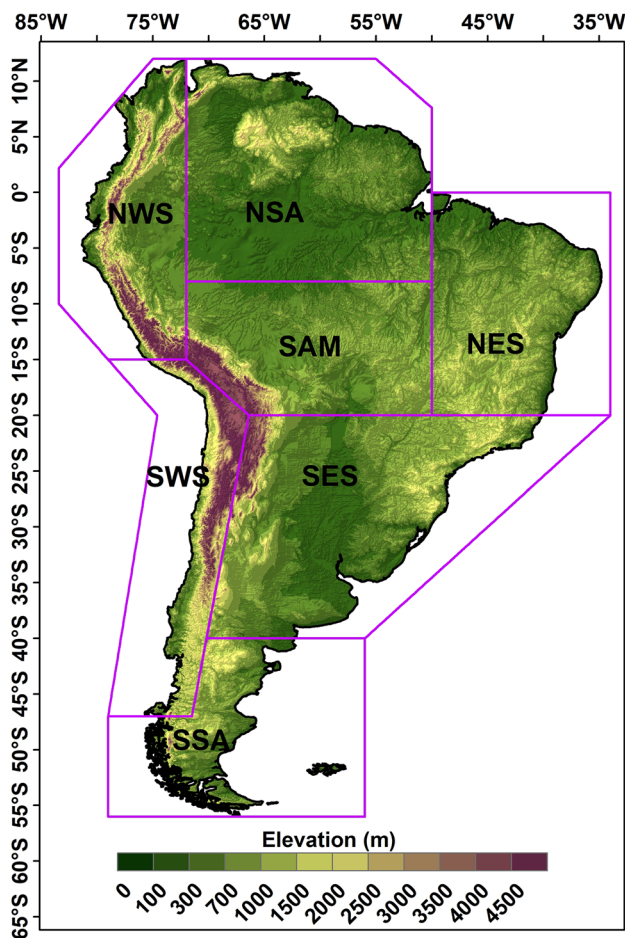
Fig. 1 South American topography and seven sub-regions used in the analyses

using their Probability Density Function (PDF) over each sub-region. PDF basic theory can be found in Forbes et al. (2011). Here, PDFs were constructed by sorting all monthly data points in space and time (time × lat × lon) in terms of their magnitude and then by partitioning those sorted values into 25 bins. GCM biases of mean and amplitude in the reference period, and GCM sensitivities in the two future periods, were evaluated using regionally averaged precipitation versus temperature scatter plots. For the reference period, the ensemble mean, each of the 38 individual GCMs, and three observation datasets (that had data for both temperature and precipitation) were averaged over each sub-region for a total of 42 data points (38 GCMs, GCM ensemble mean and 3 observation values). These were normalized with respect to the mean and standard deviation across the sample space. The same procedure was used for the future time slices just for the model data. While the normalized ensemble mean in the future periods is zero, its normalized value is non-zero in the historical period due to the presence of three observation datasets.

Lastly, we tested the robustness of projected annual and 6-monthly changes by identifying those grid points where (i) the sign of change was similar in at least 66% of the models, (ii) the magnitude of change was greater than the baseline variability (i.e., one standard deviation) in at least 66% of the models, and (iii) the magnitude of change was greater than twice the baseline variability in at least 66% of the models. The standard deviations were computed at annual and 6-month timescales to correspond to the mean temperature and precipitation values.

3 Results and Discussion

3.1 Reference Period (1994–2015) Comparisons

Except for the Patagonian Steppe in Argentina, Atacama Desert in Chile, arid coastal region in Peru, and semiarid northeast Brazil, most regions in South America receive annual precipitation > 2 mm/day (Fig. 2a, b). Precipitation patterns generally exhibit a northwest-southeast orientation over the continent due to the South Atlantic Convergence Zone (SACZ; Silva Dias and Carvalho 2017; Llopart et al. 2020a), which is the main feature of the South American Monsoon System (SAMS) variability over tropical South America in its wet season. The local convection and the onshore moisture transport from the tropical-subtropical Atlantic (Durán-Quesada et al. 2012) are important drivers for SACZ occurrence (e.g., Muñoz et al. 2015). Topographical influences on the distribution of precipitation are also well known over tropical/subtropical regions (Chavez and Takahashi 2017; Ashfaq 2020). Over South America, the Andes play an important role in maintaining the South American Low-Level Jet (SALLJ) on their east, which is an important mechanism for transporting warm and moist air from the tropics to the subtropics (Vera et al. 2006; Doss-Gollin et al. 2018; Montini et al. 2019; Kumar et al. 2020; Chavez et al. 2020).

While precipitation maxima occur over the northwest (> 12 mm/day) during April to September, it is a relatively dry season in many other parts of South America (Fig. 2g, h). During October to March, the SAMS develops over the continent and leads to a broad maximum of precipitation stretching from western Amazonia to southeastern Brazil (> 9 mm/day) (Fig. 2d, e). Considerable uncertainty (up to > ± 2 mm/day) exists among the observations with CMAP as the driest and PERSIANN as the wettest at the annual timescale (Fig. S1). Spatially, observations disagree most over the northwestern and southern parts of South America (Fig. S1). Most of the observed characteristics of precipitation are captured reasonably well in the GCM ensemble mean, particularly for April to September (Fig. 2g–i). However, the strength of the maxima over Amazonia and the

Fig. 2 Precipitation distribution (mm/day) in the ensemble mean of 8 observational datasets (first column), CRU observations (second column), and ensemble mean of 38 GCMs (third column): **a–c** annual, **d–f** October–March, **g–i** April–September. Precipitation amplitude, defined as the difference between the wettest and the driest climatological monthly means in the **j** ensemble mean of 8 observations, **k** CRU observations and l ensemble mean of 38 GCMs. These analyses are based on the 1995–2014 reference period
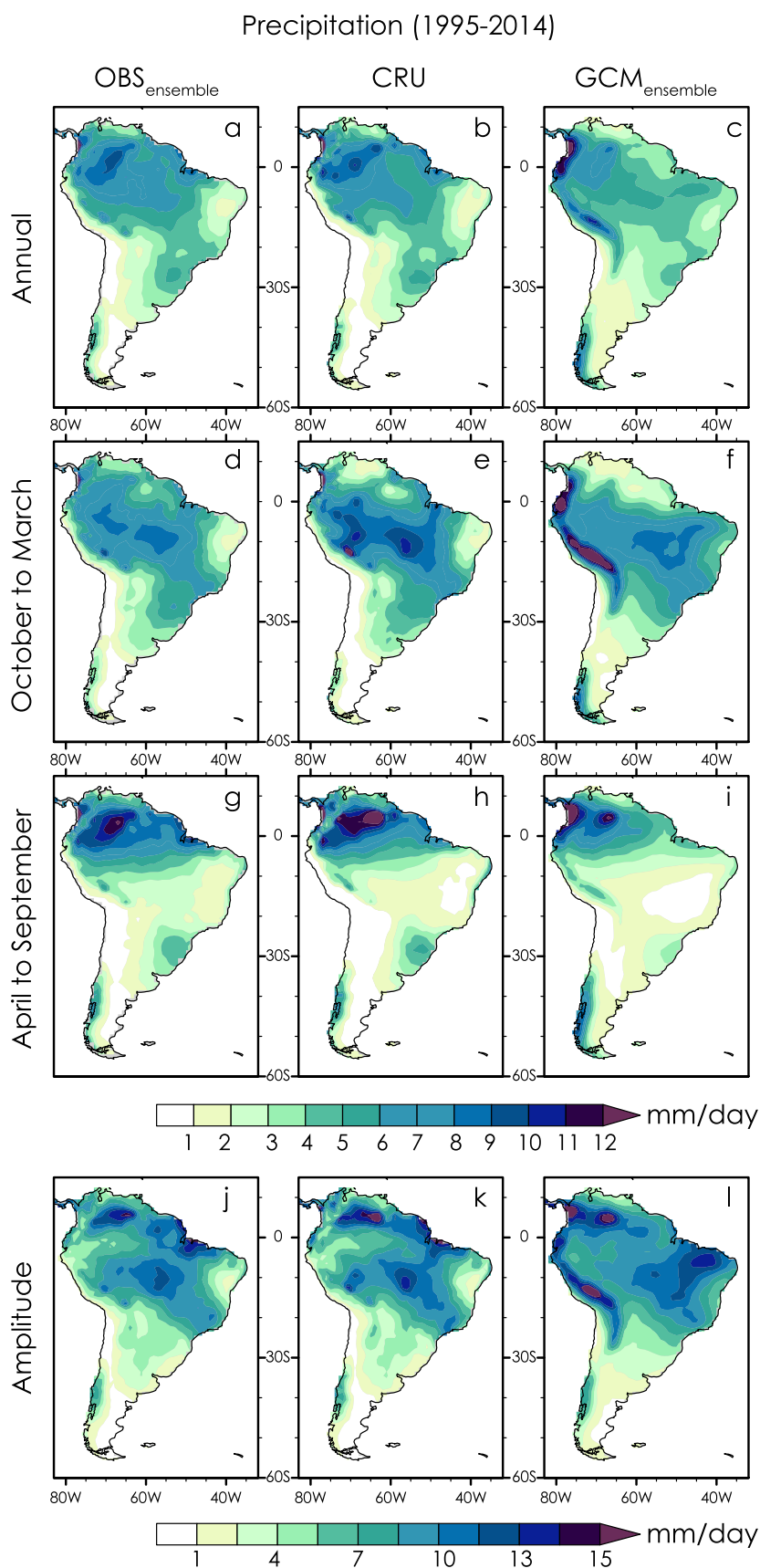
rainfall magnitudes in the La Plata basin during the two 6-months periods are much weaker, which lead to a dry bias at annual timescale (Figs. 2c, f, i, S1). This deficiency in the distribution of precipitation was also observed in the CMIP5 models and downscaled regional climate simulations (e.g., Yin et al. 2013; Gulizia and Camilloni 2015; Sánchez et al. 2015; Sierra et al. 2015; Falco et al. 2019; Llopart et al. 2020a; Ortega et al. 2021). GCMs also tend to produce overly strong precipitation over the central Andes in Bolivia, Peru, Ecuador and southwestern Colombia (Figs. 2, S1). While such excessive precipitation during the warm half of the year may be a result of overly strong convection or lack of topographic heterogeneity in the models (Chou et al. 2014), part of this disagreement can also be due to the lack of ground stations in the mountainous regions (see difference between gauge-based and satellite-based observations; see

Fig. S1), as has been noted in many earlier studies (Baez-Villanueva et al. 2018; Zubieta et al. 2019; Condom et al. 2020). Precipitation exhibits strong seasonality over the northern half of the continent, which is reflected in the large magnitude of its annual range (Fig. 2j, k). The GCM ensemble generally captures the spatial distribution of these intra-annual precipitation characteristics except for precipitation amplitudes over the Andes (Fig. 2l).

The warmest annual temperatures occur over the equatorial belt (up to 30 °C) while the southernmost zone in Chile experiences the coldest annual temperatures (below 8 °C) (Fig. 3a, b). The intra-annual temperature range exhibits characteristics opposite to those of the intra-annual precipitation range, with the weakest variations over the equatorial belt and Amazonia (< 3 °C), and the strongest variations over the transition region between the Pampas and Patagonia

Fig. 3 Annual temperature distribution (ºC) in the **a** ensemble mean of 8 observational datasets, **b** CRU observations and **c** ensemble mean of 38 GCMs. Temperature amplitude (ºC), defined as the difference between the hottest and the coldest climatological monthly means in the **d** ensemble mean of 8 observations, **e** CRU observations, **f** ensemble mean of 38 GCMs. These analyses are based on the 1995–2014 reference period

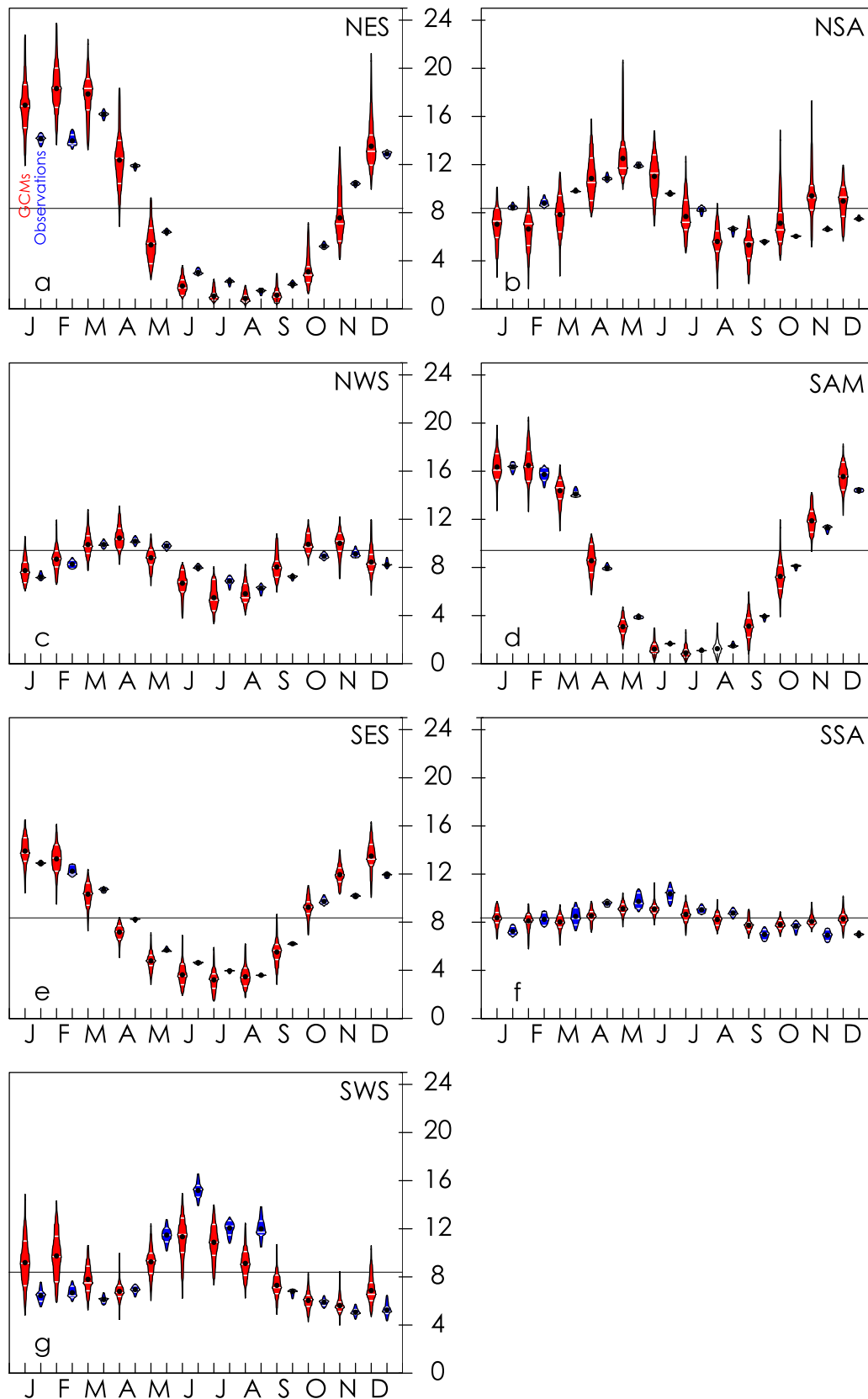Monthly Precipitaion as a Percentage of Annual Total (1995-2014)
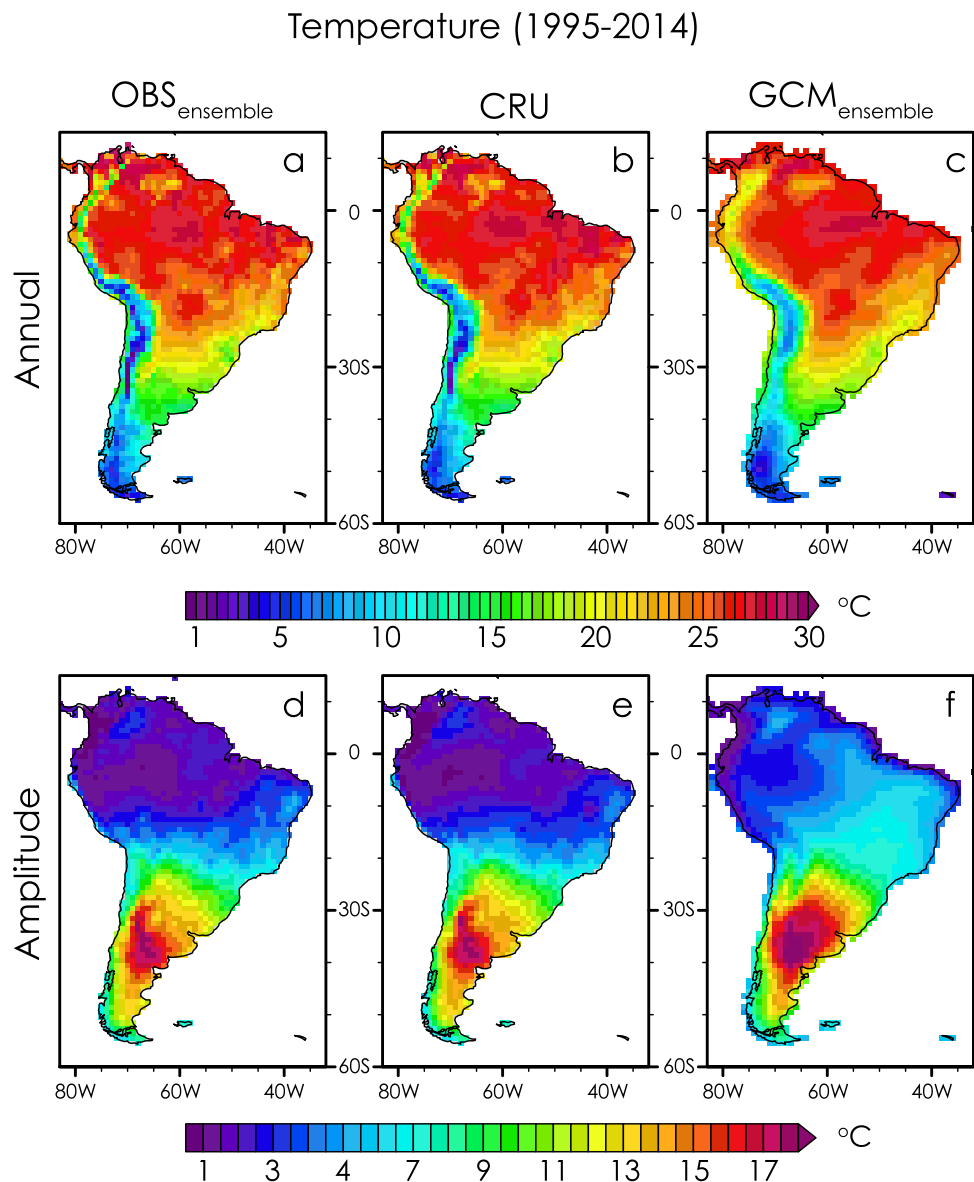
◄**Fig. 4** Monthly precipitation as a percentage of annual total over seven sub-regions based on the 1995–2014 reference period, shown as box percentiles for GCMs (38) and observations (8) ensemble. The white horizontal lines represent the 25th, 50th and 75th percentile while black dot represents the mean. The shape of the box describes the distribution of data across the ensemble members. The horizontal gray line represents percentage (8.33%) if precipitation is equally distributed across all the months. Note that CHIRPS data is excluded from the SSA region as this data does not fully cover it

(up to 18 °C) (Fig. 3d, e). Large discrepancies (up to ± 3 °C) exist among the observations, with CRU as the warmest over the eastern half and UoD as the coldest at the annual time-scale (Fig. S2). Observations also exhibit differences along the Andes, which may partly be due to their resolution differences (Fig. S2). Understandably, compared to precipitation, GCMs are relatively more skillful in the simulation of mean annual temperatures and their intra-annual range (Figs. 3, S1). However, they have a strong bias along the Andes (Fig. 3c), which is partly due to the poor representation of highlands in coarse resolution GCMs (Bozkurt et al. 2019; Pabón-Caicedo et al. 2020; Arias et al. 2021b; Ortega et al. 2021).

GCM performance in reproducing the spatially averaged annual cycle of precipitation over the seven sub-regions has been analyzed and compared with observations as box percentiles (Fig. 4). The annual cycle of monthly precipitation, expressed as percentages of the annual total, shows heterogeneity at both regional and temporal scales. In the northeast (NES), southern Amazonia (SAM) and southeast (SES) sub-regions (Fig. 4a, d, e), the months from October to April make the largest contribution to the annual total of precipitation (up to 16% per month), while May to September months add smaller fractions (below 6% per month). Given the strong seasonality of precipitation, this division can be referred to as the wet and dry periods, respectively, over these sub-regions. Overall, the GCM ensemble mean (black dots in Fig. 4) for NES, SAM and SES sub-regions display good agreement with observations. However, it is worth highlighting that the simulated magnitudes over these sub-regions are overestimated during the wet period, while underestimated during the dry period. The spread across the GCMs is also high during the wet season, as by shown the width of the shapes in Fig. 4. The observed pattern and the corresponding bias in the GCM ensemble for the southwest (SWS) sub-region are diametrically opposite to the previously mentioned sub-regions, since the precipitation peak (> 16% of annual totals in one month) is observed during the austral winter. Moreover, the GCM ensemble not only underestimates the contribution during the peak precipitation months (and overestimates it during the dry months), it also exhibits substantial spread (up to ± 4%) across the mean. The northern (NSA) and northwestern (NWS) sub-regions show an annual cycle with bimodality of precipitation, while

it is quite uniformly distributed across the months over the southern (SSA) sub-region (Fig. 4b, c, f). Sub-regional averages are not necessarily representative of the precipitation seasonality within an area if it exhibits strong spatial heterogeneity in climate characteristics, as in the NWS case where intra-annual variability of precipitation is clearly smoothed out. The NWS sub-region exhibits distinct climate characteristics both from west to east, including an arid coastal strip, the wetter Andes (or the Sierra region) and the tropical forest region of Peruvian Amazon, and from north to south, including equatorial climate in Ecuador and Colombia and subtropical climate in the southernmost limit of the region (Espinoza et al. 2020). Overall, the GCM ensemble captures these principal characteristics of precipitation over these sub-regions, as also highlighted by Ortega et al. (2021). However, substantial spread across the mean exists among the models over NSA throughout the year (Fig. 4b). Some disagreement among observations is also noticeable in the southern sub-regions (SSA, SWS).

The correspondence of individual GCM and three observations (CRU, UoD, TerraClimate) at regional scale has been further analyzed in the normalized precipitation versus temperature plots for the reference period (1995–2014) (Fig. 5). The distance of (i) individual GCM (black) from the ensemble mean (red), (ii) the ensemble average and individual GCM from observations (UoD: green; CRU: blue; TerraClimate: purple), and (iii) one observation from others are the three aspects that respectively provide insight into the models' agreement among themselves, their agreement with the observations, and the uncertainty in observations. GCMs within 1 standard deviation (SD) along the two axes (blue dashed center square) can be considered as the ones relatively closer to the mean, while those outside of the 2 SD along the precipitation or temperature axis can be identified as outliers in that dimension (pink). Likewise, the location of three observations on the XY map provides insight into their agreement with the numerical solutions. The strongest agreement between the observations and simulations is observed over the SAM and SES regions where observations are close to the ensemble mean. The strongest disagreement between the observations and simulations occurs over SSA along the precipitation axis where all models are significantly wetter than the observations, and over SWS where models are not only significantly wetter but also warmer than the observations. Alternatively, a majority of the GCMs tend to be relatively drier over NSA and drier and colder over NES compared to the observations. The largest spread across the GCMs along each axis is seen over the NES sub-region, while the NSA sub-region exhibits the maximum number of outliers (pink). Overall, these comparisons highlight the fact that there are a number of sub-regions across South America where GCMs either have robust biases relative to the observations or display significant disagreements among

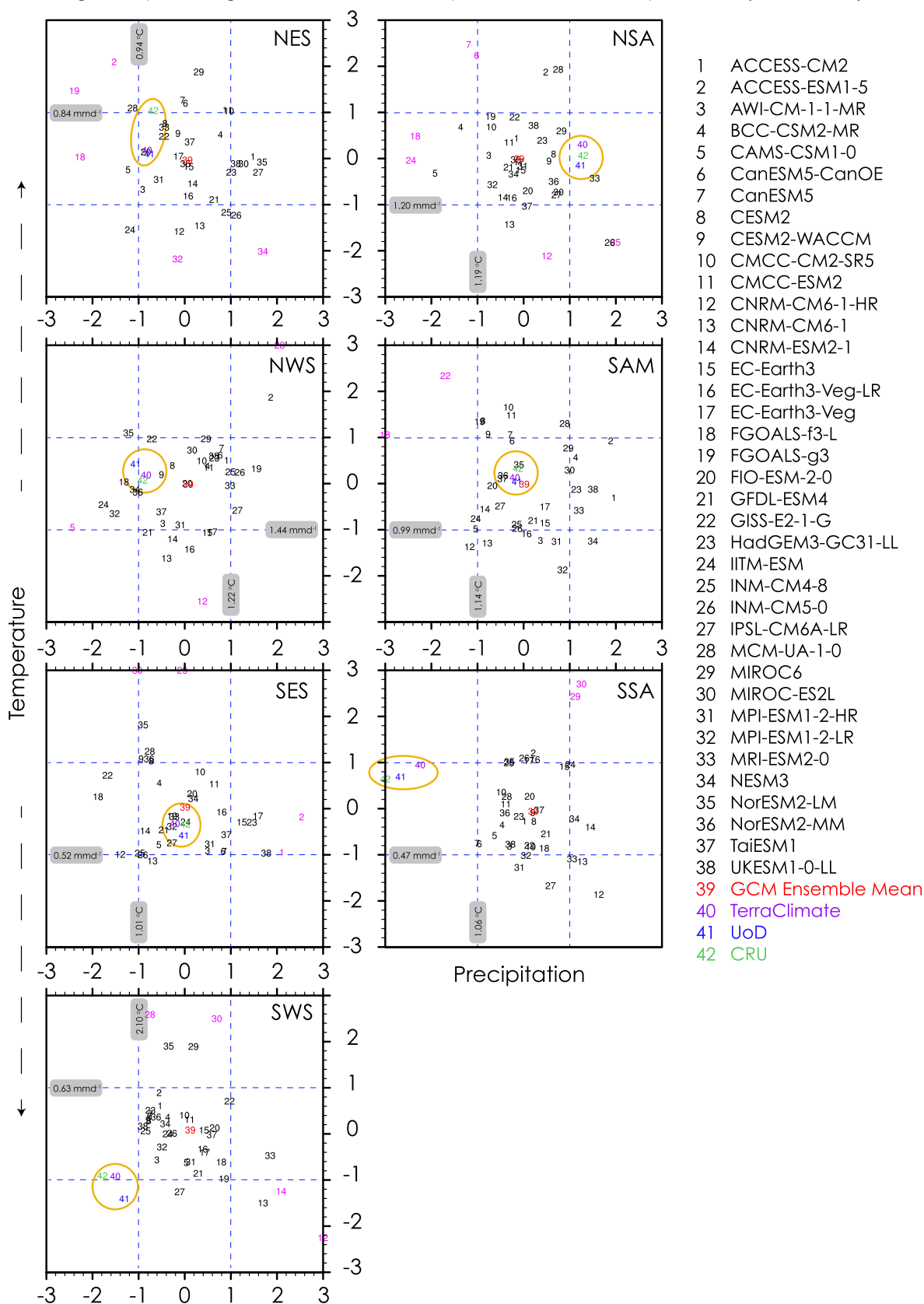Regionally Averaged Normalized Precipitation versus Temperature (1995-2014)

1	ACCESS-CM2
2	ACCESS-ESM1-5
3	AWI-CM-1-1-MR
4	BCC-CSM2-MR
5	CAMS-CSM1-0
6	CanESM5-CanOE
7	CanESM5
8	CESM2
9	CESM2-WACCM
10	CMCC-CM2-SR5
11	CMCC-ESM2
12	CNRM-CM6-1-HR
13	CNRM-CM6-1
14	CNRM-ESM2-1
15	EC-Earth3
16	EC-Earth3-Veg-LR
17	EC-Earth3-Veg
18	FGOALS-f3-L
19	FGOALS-g3
20	FIO-ESM-2-0
21	GFDL-ESM4
22	GISS-E2-1-G
23	HadGEM3-GC31-LL
24	IITM-ESM
25	INM-CM4-8
26	INM-CM5-0
27	IPSL-CM6A-LR
28	MCM-UA-1-0
29	MIROC6
30	MIROC-ES2L
31	MPI-ESM1-2-HR
32	MPI-ESM1-2-LR
33	MRI-ESM2-0
34	NESM3
35	NorESM2-LM
36	NorESM2-MM
37	TaiESM1
38	UKESM1-0-LL
39	GCM Ensemble Mean
40	TerraClimate
41	UoD
42	CRU

◄**Fig. 5** Normalized precipitation versus temperature maps over seven sub-regions based on the 1995–2014 reference period. The GCM ensemble mean, 38 individual GCMs, and two observational datasets are averaged over each region and 41 data points are normalized with respect to the mean and standard deviation across the sample (temperature/precipitation) space. The dotted blue lines represent 1 standard deviation (SD) along each axis. The magnitudes of precipitation (horizontal axis) and temperature (vertical axis) standard deviations are shown in gray boxes. Values shown as pink are the ones that are at a distance of 2 SD from the center and can be considered outliers. Any value greater than 3 SD is shown as 3 SD. The yellow ovals highlight the location of observations. The ovals in each panel represent locations of three observational datasets

themselves in the CMIP6 ensemble, which is also observed for seasonal precipitation by Ortega et al. (2021). We also note disagreement among observations over SWS along the precipitation axis, and over NES along the temperature axis, which is understandable through the differences in the precipitation and temperature maps over these sub-regions (Figs. S1, S2).

We also evaluate the GCM skill in the spatiotemporal distribution of precipitation and temperature over each sub-region using PDFs (Sect. 2) (Figs. 6, 7). First, we note obvious differences in the distribution of precipitation among observations over several sub-regions (Fig. 6). For instance, the frequency of months with precipitation ≤ 20 mm/day, ≤ 10 mm/day and ≤ 4 mm/day is substantially higher in PERSIANN over NWS, NES and SSA respectively, which explains its wetter tendency over these sub-regions (Fig. S1). Similarly, CRU exhibits noticeably higher frequency of months with ≤ 12 mm/day over SAM. The average PDF (red) based on the mean of PDFs of all GCMs compares well with most of the observations, with the significant exceptions of NSA and SES for the low intensity months (≤ 3 mm/day; Fig. 6b, e) and SSA, NWS, SWS for the medium to high intensity months (≥ 3 mm/day; Fig. 6f), which are more frequent in the simulated ensemble mean in both cases. The spread across the GCMs is relatively large over the NSA, NWS, SAM and SES sub-regions (Fig. 6b-e), as has also been partly reported in Diaz et al. (2021).

Compared to the precipitation PDFs, temperature observations are in relatively better agreement in terms of their monthly distribution, with a few exceptions over NES and SWS, where the temperature in the coldest months tends to be warmer in CRU compared to other observations (Fig. 7). Disagreements also exist among observations in the frequency of the modal value over NSA and SES (Fig. 7b, e). The average PDF based on all GCMs captures the magnitude and frequency of tail months (warmest and coldest) in agreement with the majority of observations over most sub-regions, with some noticeable exceptions mostly in the case of warm months over NSA, SAM and SWS (Fig. 7b, d, g). The mean and the individual GCM PDFs tend to differ more from the observations in the center of the distribution

with most prominent deviations over NES, NWS and SSA (Fig. 7a, c, e). Overall, these comparisons of precipitation and temperature reflect the large spatio-temporal climate variability over South America and highlight the fact that GCM errors grow at regional scales.

3.2 Projected Spatial Changes in Temperature and Precipitation

Earlier projections using CMIP5 GCMs suggested a decrease in precipitation east of the northern Andes in tropical South America, over the southern Andes in Chile and Amazonia, and an increase in precipitation over southeastern South America and the northern Andes (Gulizia and Camilloni 2015; Palomino-Lemus et al. 2015, 2017; Zazulie et al. 2018; Llopart et al. 2020a; Parsons 2020; Sena and Magnusdottir 2020; Arias et al. 2021b; Ortega et al. 2021; Thaler et al. 2021). The changes are larger and more robust in the higher emission pathway (RCP8.5) compared to the lower emission pathway (RCP2.6) (Riahi et al. 2011; Ortiz-Jiménez 2018). The spatial signals in the projected precipitation changes in the CMIP6 GCM ensemble, used in this study, are consistent with the CMIP5 GCM projections, with the exception that eastern tropical South America now exhibits a positive change (Fig. 8). The projected changes progress monotonically from the weakest (SSP126) to the strongest (SSP585) forcing scenario, and from the mid-century (2040–2059) to the late-century (2080–2099) projection period.

In the mid-century (Fig. 8), a robust (in terms of sign) reduction in mean annual precipitation appears over parts of the central tropical belt and over central-southern Chile, while robust (in terms of sign) increases are exhibited over southeastern South America. The patterns of changes are consistent in both wet and dry season precipitation over these regions though the robust reduction over the tropical belt expands over Brazil during the dry season (Fig. 8i–l). The changes not only become stronger in magnitude but also spatially more robust across the CMIP6 GCMs when increasing the strength of the forcing (Fig. 8a, e, i versus Fig. 8d, h, l). The range of precipitation increases over most of the continent (Fig. 8m–p) with a few exceptions over central-southern Chile and parts of the equatorial belt. These changes in the annual precipitation amplitudes suggest that, across South America, the relative contribution to the annual mean increases during the wettest months while it decreases during the driest months, which is explained further in subsequent analyses (subsection 3.4).

The spatial pattern of precipitation change persists in the late-century future (2080–2099) (Fig. 9). The changes mostly differ in magnitude, as they become stronger in the late-century period, which suggests a potentially simple proportional scaling with increased radiative forcing. It

Fig. 6 Probability density function of monthly precipitation over each sub-region in the reference period. Each sub-regional probability distribution was generated by dividing all monthly land data points in space and time (time×lat×lon) in 25 bins

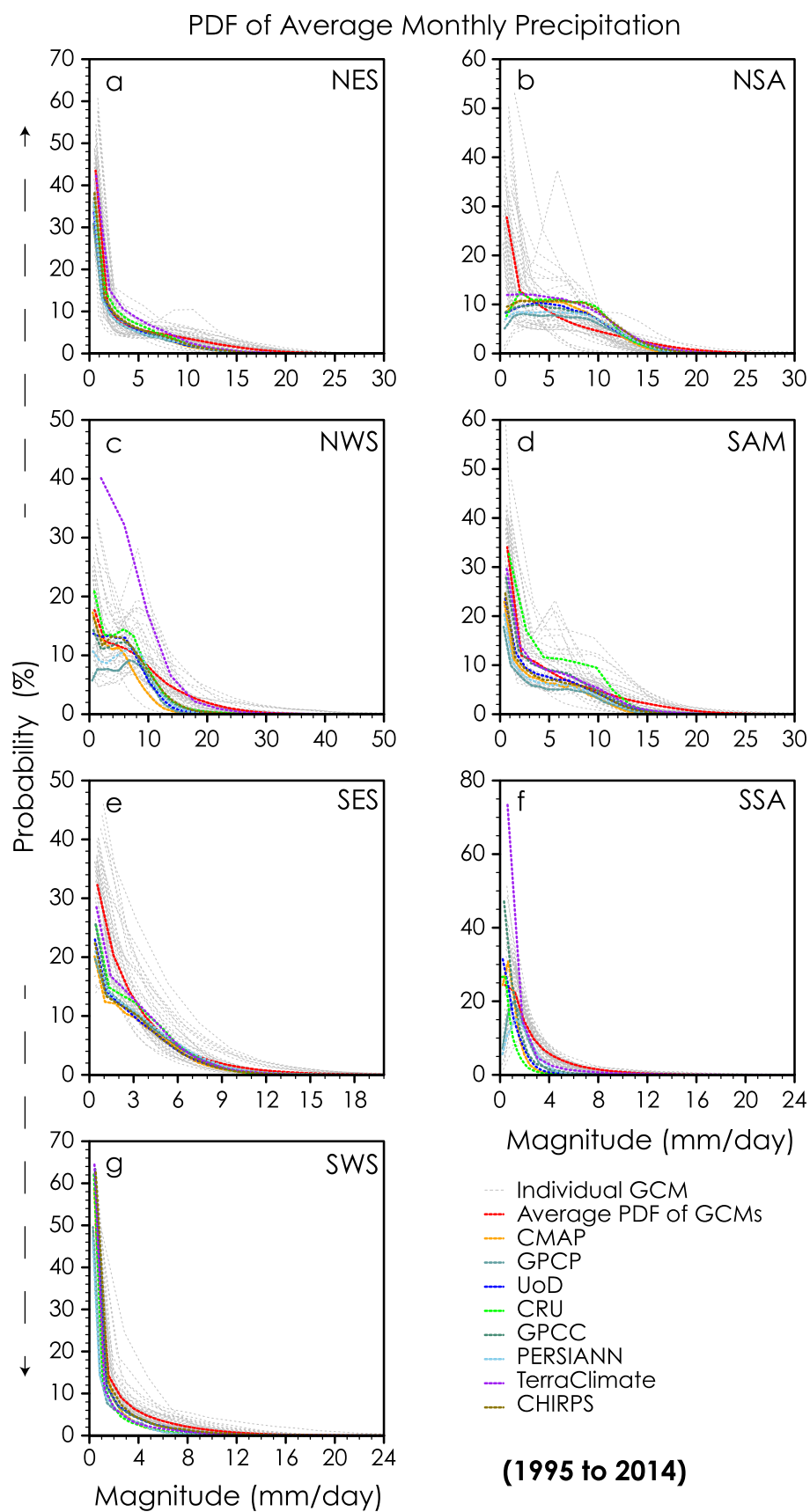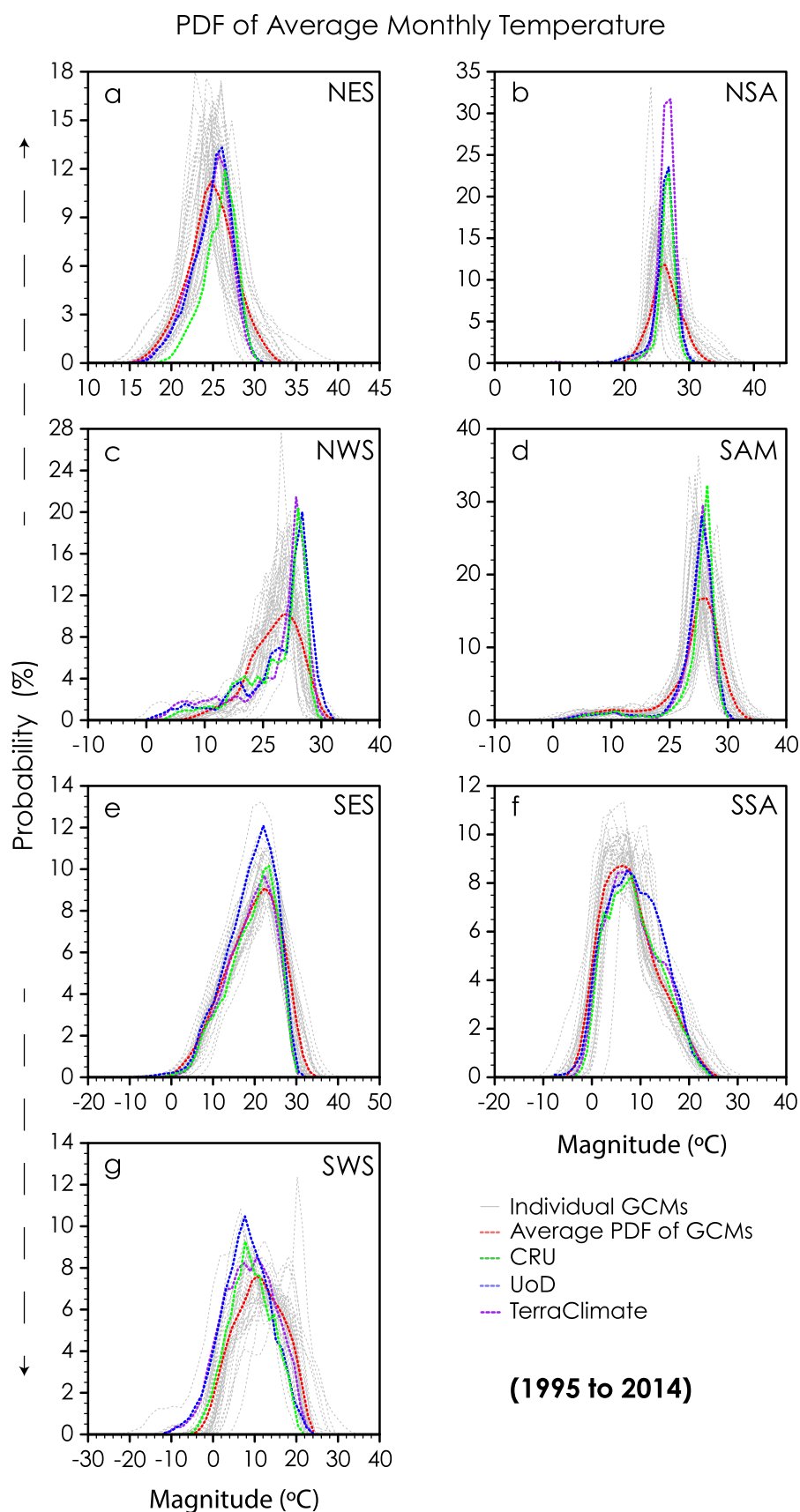PDF of Average Monthly Precipitation

Probability (%)

Magnitude (mm/day)

Individual GCM
Average PDF of GCMs
CMAP
GPCP
UoD
CRU
GPCC
PERSIANN
TerraClimate
CHIRPS

(1995 to 2014)

Fig. 7 Same as in Fig. 6 but for monthly temperature

PDF of Average Monthly Temperature

(1995 to 2014)

— Individual GCMs
— Average PDF of GCMs
— CRU
— UoD
— TerraClimate

Precipitation Change (2040-2059 w.r.t. 1995-2014)

Annual Precipitation Amplitude Change (2040-2059 w.r.t. 1995-2014)
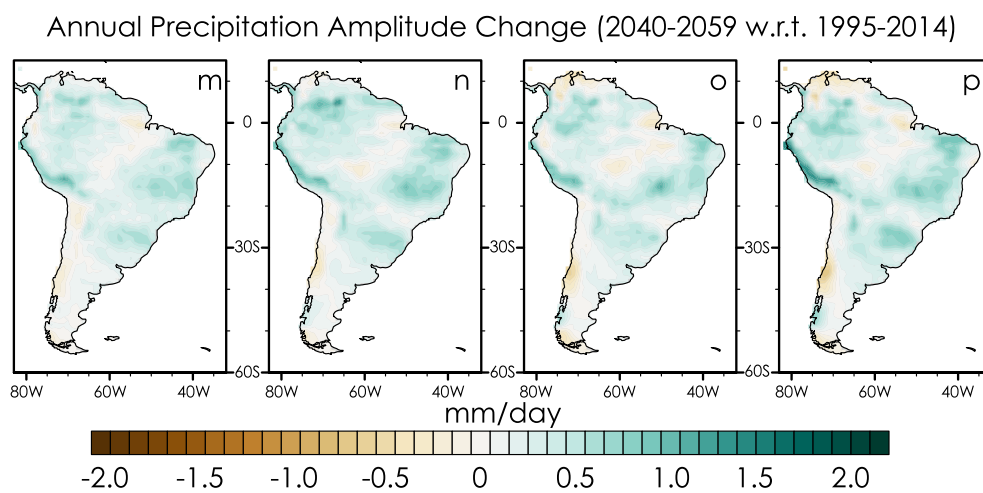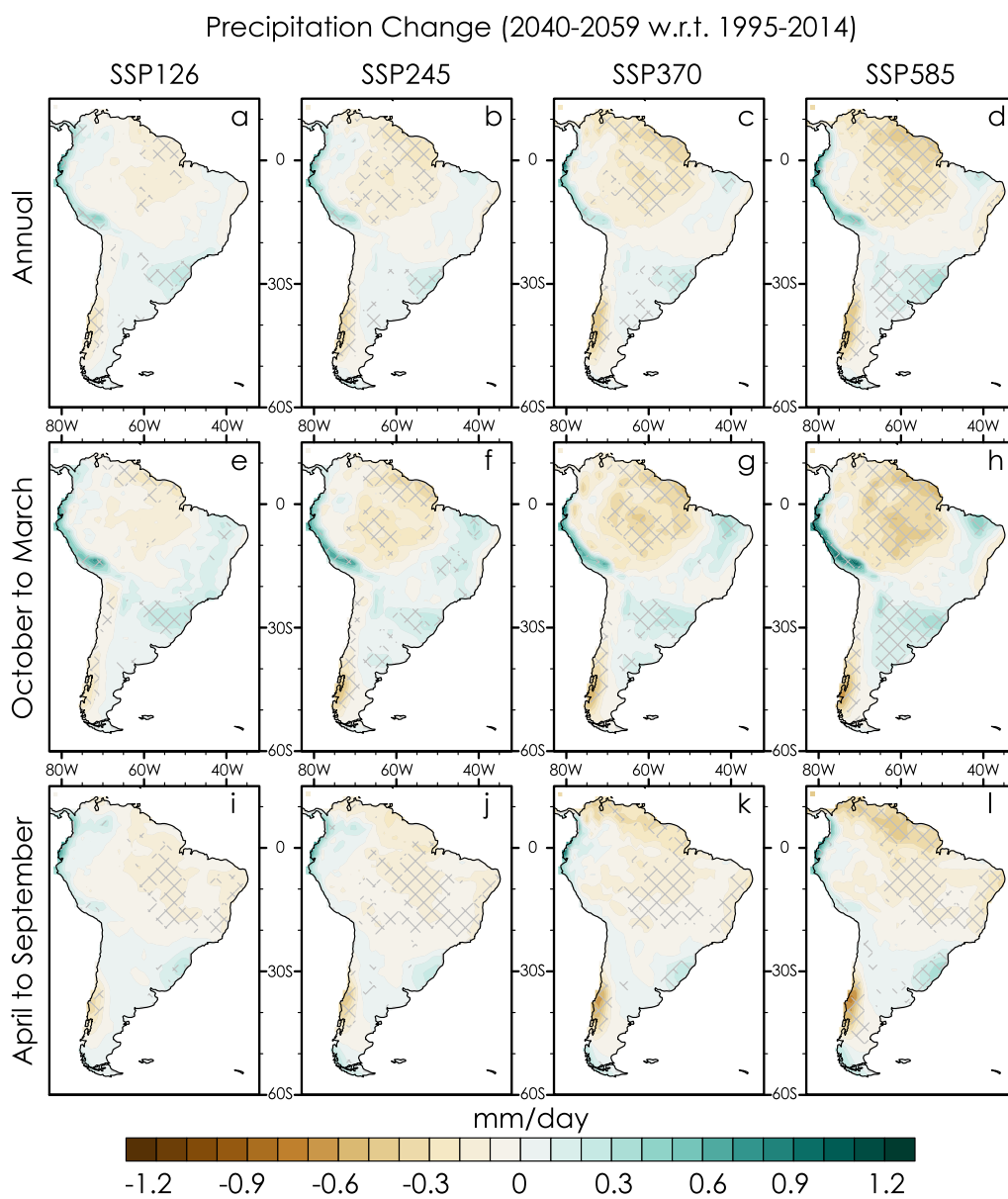
◀**Fig. 8** Precipitation change in the mid-century future (2040–2059; mm/day) with respect to the reference period (1995–2014) under all four future scenarios **a–d** annual, **e–h** October–March, **i–l** April–September. Gray stippling represents the regions where projected changes are robust in terms of the sign of change, meaning that at least 66% of GCMs agree on the sign of precipitation change. Mid-century changes in the precipitation amplitude (m-p; mm/day) in all four future scenarios. All changes in amplitude are robust in terms of the sign of change

is important to note that future precipitation change only starts becoming greater than the baseline variability (i.e., robust in terms of magnitude) in SSP370 and SSP585 in the late-century period. All other precipitation changes in the mid-century period under all future scenarios and in the late-century period under SSP126 and SSP245 are within the baseline variability (Figs. 8, 9) and therefore not robust in terms of magnitude. In SSP370, change greater than the baseline variability is limited to parts of central-southern Chile in the dry season (Fig. 9g). In SSP585, in addition to the central-southern Chile region, the decrease over the parts of the Amazon and central tropical belt also becomes greater than the baseline variability (Fig. 9d, h). The relative disparity between the driest and wettest months also grows in the future period with the exceptions of parts of central-southern Chile and the tropical belt (Fig. 9m-p). Both regions exhibit decreases throughout the year. However, the relative decrease in the wetter months is larger than that in the drier months. These results are consistent with earlier studies (Pendergrass et al. 2017; Alves et al. 2020; Llopart et al. 2020b; Ortega et al. 2021).

In contrast to precipitation changes, temperature changes are robust both in terms of sign and magnitude even for the lowest emission scenario SSP126 (Fig. 10). Average annual temperature increases in the mid-century period range between 0.5 and 1.5 ºC in SSP126, 1.0–1.8 ºC in SSP245, 1.0–2.4 ºC in SSP370, and 1.2–3.0 ºC in SSP585, respectively. While there is not much further increase in temperature under SSP126 towards the end of the century, other future scenarios exhibit substantially more warming, ranging between 1.7 and 3.0 ºC in SSP245, 2.2–4.4 ºC in SSP370, and 2.8 to > 5.0 ºC in SSP585, especially over the tropical regions (NAS, SAM, NES). All these temperature increases are greater than twice the baseline variability (white dots) with the exception of SSP126, where such increases are mostly limited to the central parts of the continent. Note that the strongest warming across all future scenarios is over the Amazon. The disparity between warmest and coldest months also exhibits an increase across all scenarios, meaning that warming is predominantly driven by warm season changes (Fig. 10i–p). However, the magnitude of these increases only starts becoming robust (greater than baseline variability; Fig. 10) towards the end of the century in SSP370 and SSP585 (black and white dots). The disparity is strongest

over the Amazon and southern Andes, and is greater than the baseline variability over parts of Amazon in SSP370 (Fig. 10o) and greater than twice the baseline variability throughout the continent in SSP585 (Fig. 10p).

3.3 Spatiotemporal Distribution of Projected Changes in Temperature and Precipitation

We also examined the spatiotemporal distribution of precipitation and temperature changes across all months and grid points over each sub-region in the two projection periods (Figs. 11, 12). Several important characteristics of changes can be revealed through these comparisons. First, the distribution of precipitation over most of the regions is skewed left, with the exception of SES where it is skewed right (Fig. 11e) and NWS where it is almost symmetrical (Fig. 11c). The left skewed PDFs suggest that mean and median of the distribution are smaller than the mode or most common data point (zero in this case) and vice versa, which is understandable given that net precipitation change is negative over all sub-regions except SES and parts of NWS (Figs. 8, 9). The skewness of the PDFs increases in the late twenty-first century period as precipitation changes intensify. The largest difference between the mid-century and late-century projection periods in terms of leftward skewness is over NSA, followed by SAM and SWS in SSP370 and SSP585 (Fig. 11b, d, g). The relatively high probability of extremes in the late-century future suggests that monthly precipitation anomalies that are rare in the historical climate become commonplace by the end of the twenty-first century, consistent with earlier CMIP5-based findings (Alves et al. 2020). Over most sub-regions, this change in monthly precipitation distribution is related to negative anomalies, while over NWS it accounts for both negative and positive anomalies (Fig. 11c), and over SES it is related to the positive anomalies (Fig. 11e). Interestingly, the smallest regionally averaged precipitation changes are over NWS, which contrasts with the fact that this sub-region exhibits an increase in both wet and dry monthly extremes. Indeed, it is the compensating impact of equally distributed wet and dry monthly anomalies over NWS that mutes the overall regionally averaged precipitation change, which highlights the limitations of area averaged precipitation change in understanding regional climate change.

In the case of monthly temperatures, almost all the months and grid points across all regions exhibit a positive change (Fig. 12). In contrast to the precipitation change distribution (Fig. 11), differences in the distribution of temperature change are visible across different scenarios even in the mid-century period. As expected, increases under SSP126 remain more or less similar between the two projection periods, while increases under SSP370 and SSP585 differ substantially in the two time periods. More importantly, the
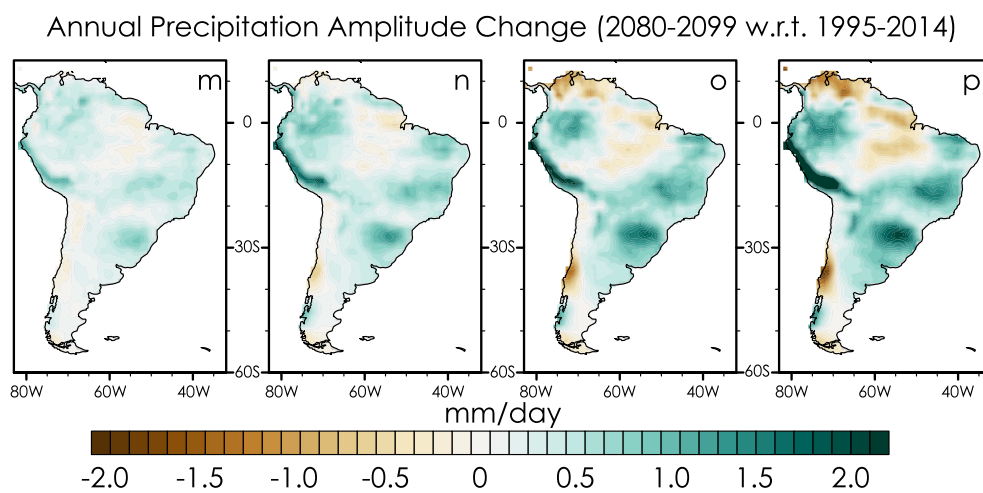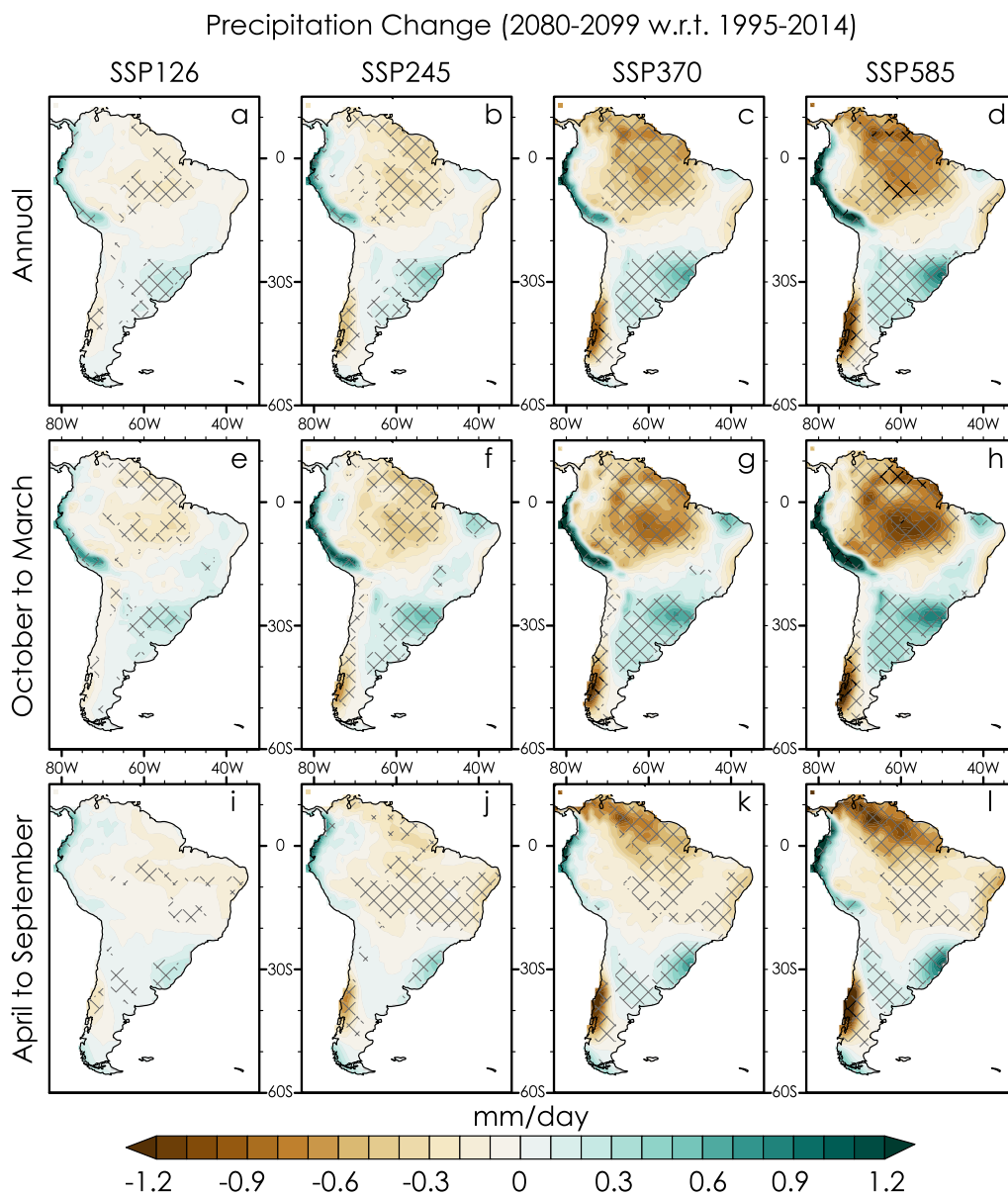
Precipitation Change (2080-2099 w.r.t. 1995-2014)

Annual Precipitation Amplitude Change (2080-2099 w.r.t. 1995-2014)

◄**Fig. 9** Same as in Fig. 8 but for the late-century future (2080–2099; mm/day). Black stippling represents the regions where projected changes are robust both in terms of sign and magnitude. The robustness in terms of magnitude is defined using the reference period standard deviation as a threshold

distribution of change in the two higher-end scenarios is mostly outside the distribution of change in the two lower-end scenarios (SSP126, SSP245).

Moreover, sub-regions comprising the northern half of the continent tend to exhibit stronger warming as the magnitude of temperature change decreases with increasing latitude in the Southern Hemisphere, consistent with earlier CMIP5-based projections (e.g., Llopart et al. 2020a). Under the highest emission scenario (SSP585), the strongest regionally averaged warming is over SAM in the late twenty-first century (5.4 °C; Fig. 12d) while the weakest warming is over SSA (3.0 °C; Fig. 12f). This temperature response is in contrast to that seen over North America where higher latitudes tend to exhibit the strongest warming signal (Almazroui et al. 2021). These contrasting latitudinal variations in temperature response over North and South America can be partly explained in terms of their differences in the characteristics of precipitation type. In contrast to South America, where significant amounts of snow are limited to higher altitudes or polar latitudes, the snow to precipitation ratio is considerably higher over middle and higher latitudes in North America, which exhibits a strong decline in response to increase in radiative forcing and leads to pronounced surface warming in the future period (e.g., Ashfaq et al. 2016).

3.4 Intra-Annual Changes in Precipitation Characteristics

As previously noted, there is increased disparity between the wettest and the driest periods of the year, as is also clear in Figs. 13 and 14, which show changes in the relative contribution of each month to annual precipitation. Months that exhibit a relatively high contribution to the annual mean tend to have an increase in the relative contribution to the annual mean over NES, NSA, NWS, and SAM. Exceptions occur over SES where the extra fractional contributions to the annual mean come in the transition months, and over SWS where results are mixed. These results suggest that regardless of the net change, precipitation is becoming more seasonal in the future climate. These changes are progressive and become stronger in the late twenty-first century and at higher forcing levels.

We also examined the spread across the GCM ensemble at sub-regional scale for future changes in spatially averaged relative contributions of monthly precipitation to annual means. (Figs. S3–S9). The comparison of intra-GCM spread in the mid-century and late-century future suggests

that disagreement among the models increases with time regardless of the future scenario. The spread is particularly large and positively skewed over NSA during the warm season and over SAM during the cold season.

3.5 Regional Uncertainty in GCM Projections

Lastly, we investigated the uncertainty across the GCM ensemble in their simulated sub-regionally averaged precipitation and temperature changes over two projection periods (Figs. 15, 16), which reveals several interesting aspects of CMIP6 GCM behavior in simulating future climatic changes. First, the precipitation and temperature response in each GCM tends to cluster in the same area on the two-dimensional space across different future scenarios, meaning that relative sensitivity of a GCM with respect to the ensemble mean does not vary substantially across different scenarios. Second, the relationship between the magnitude of precipitation change versus temperature change across the GCM ensemble apparently depends on the climate characteristics of a region. For instance, higher precipitation change is seen in GCMs with higher temperature change and vice versa over the tropical and subtropical belts of the continent (NES, NSA, NWS, SAM; Figs. 15a–d, 16a–d). In contrast, with few exceptions, in the middle to higher latitudes, such a relationship either is very weak or in reverse order, meaning that either there is no pattern in precipitation and temperature change or models with higher temperatures also tend to have higher precipitation (SSA, SWS, SES; Figs. 15e–g, 16e–g). Third, models are more in agreement towards the end of the century than in the mid-century, which is why precipitation and temperature changes are more robust in the late-century (see Figs. 9, 10). Fourth, there is no clear systematic relationship between the magnitude of GCM biases in the historical period (Fig. 4) and their sensitivity to future increases in radiative forcing (or simulated future climate change) (Figs. 14, 15).

4 Summary and Conclusions

We have evaluated a large ensemble of CMIP6 GCMs over South America for their performance in the reference period (1995–2014) and projected climate change in the mid-century (2040–2059) and late-century (2080–2099) future periods under four SSP-RCP scenarios. In the reference period, while models are able to represent the main climate characteristics across South America, they exhibit varying skill in the spatiotemporal distribution of precipitation and temperature at sub-regional scale, particularly over high latitudes and altitudes. A noticeable disparity also exists among observations throughout the continent, which highlights both the need for improvements in observational networks and the

Fig. 10 Annual temperature change (°C) in the mid-century (2040–2059; **a–d**) and late-century (2080–2099; **e–h**) futures with respect to the reference period (1995–2014) under all four future scenarios. Changes in the temperature amplitude (°C) under all four future scenarios in the mid-century (**i–l**) and late-century (**m–p**). Gray stippling represents the regions where projected changes are robust in terms of the sign of change. Black stippling represents the regions where projected changes are greater than baseline variability (1 Standard deviation; 1SD) while white dots represent the regions where projected changes are greater than twice the baseline variability (2 SD)
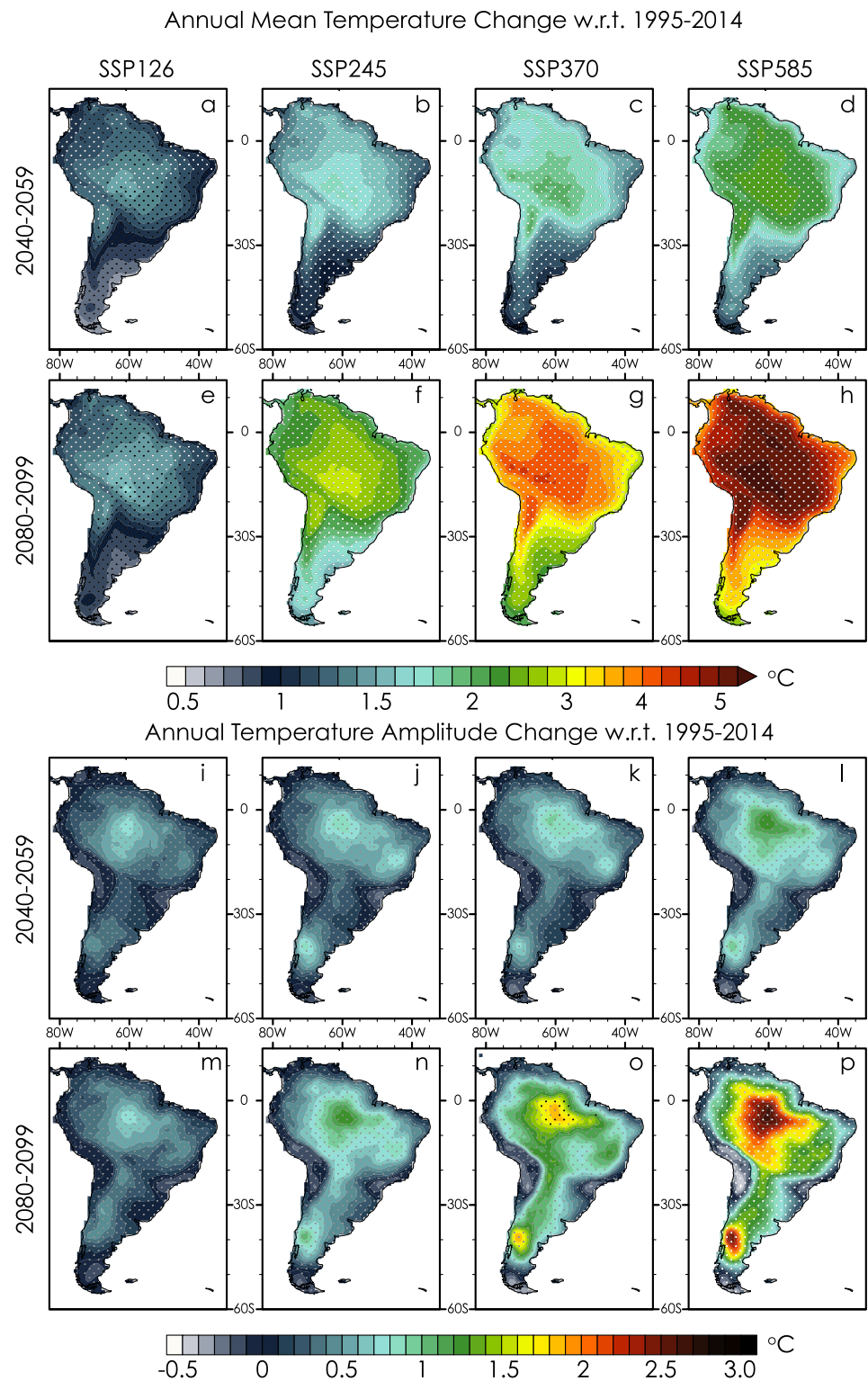
importance of the use of multiple observational products for climate studies.

Three main factors, namely the future climate forcing scenario, model structure and internal variability of the climate system, contribute to uncertainties in future climate projections (Hawkins and Sutton 2009). Our use of multiple GCMs and future scenarios addresses the first two factors. The comparison of multiple future pathways also helps to understand the benefits of limiting greenhouse gas emissions. To this end, we note that substantial change in future

Fig. 11 Probability density function (PDF) of monthly precipitation change over each region in the future periods under all four scenarios. Each regional PDF has been generated by dividing all monthly changes over each land point in space and time in 25 bins. The future changes at each grid point are based on the difference of each month from its respective monthly climatology in the reference period (1995–2014). The numbers in each plot represent regionally averaged % precipitation change in the late-century (mid-century) period

PDF of Average Monthly Precipitation Change
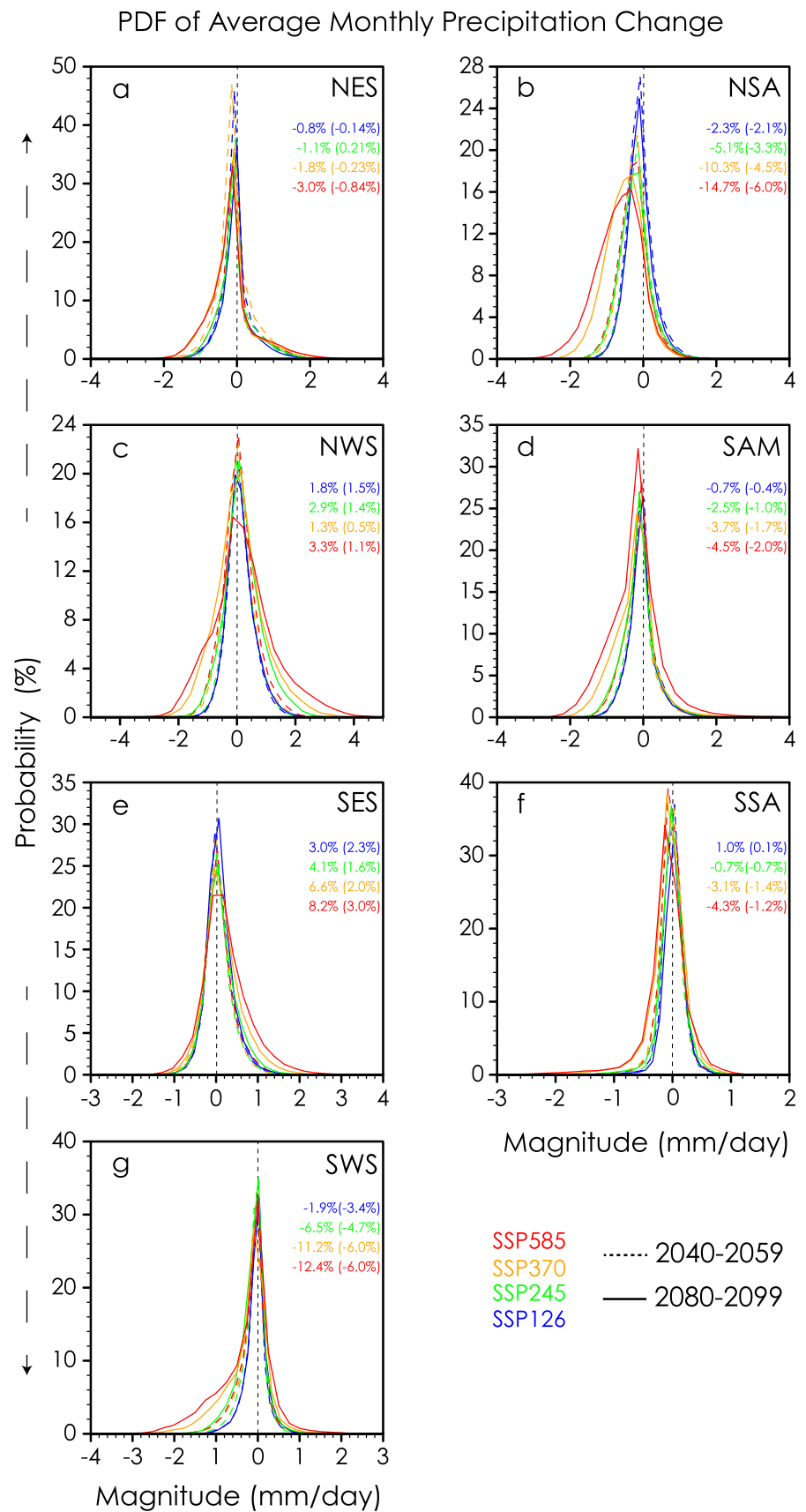
Fig. 12 Same as in Fig. 11 but for monthly temperature

PDF of Average Monthly Temperature Change

Changes in Monthly Precipitaion Fraction w.r.t Annual Total (2040-2059)
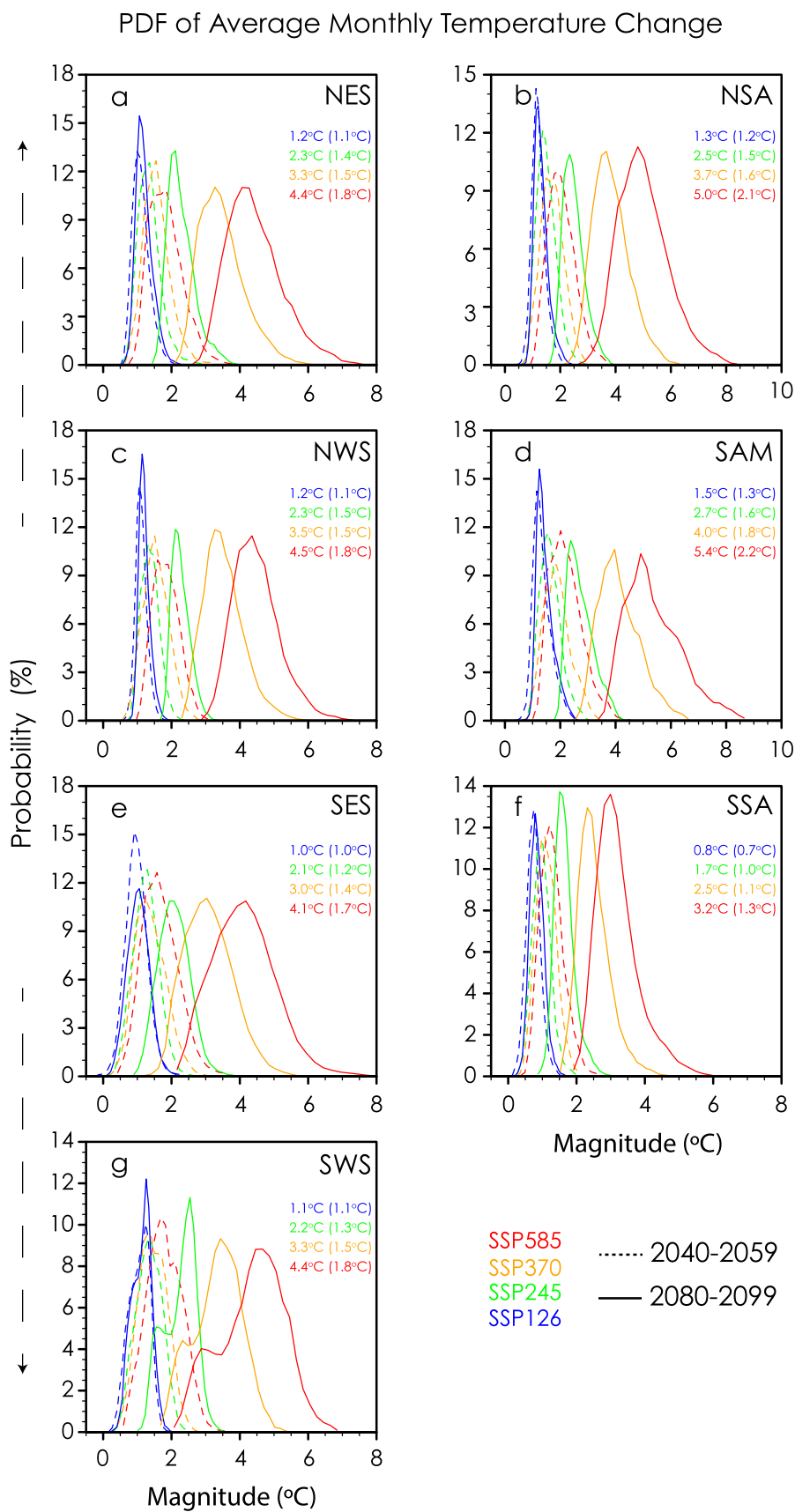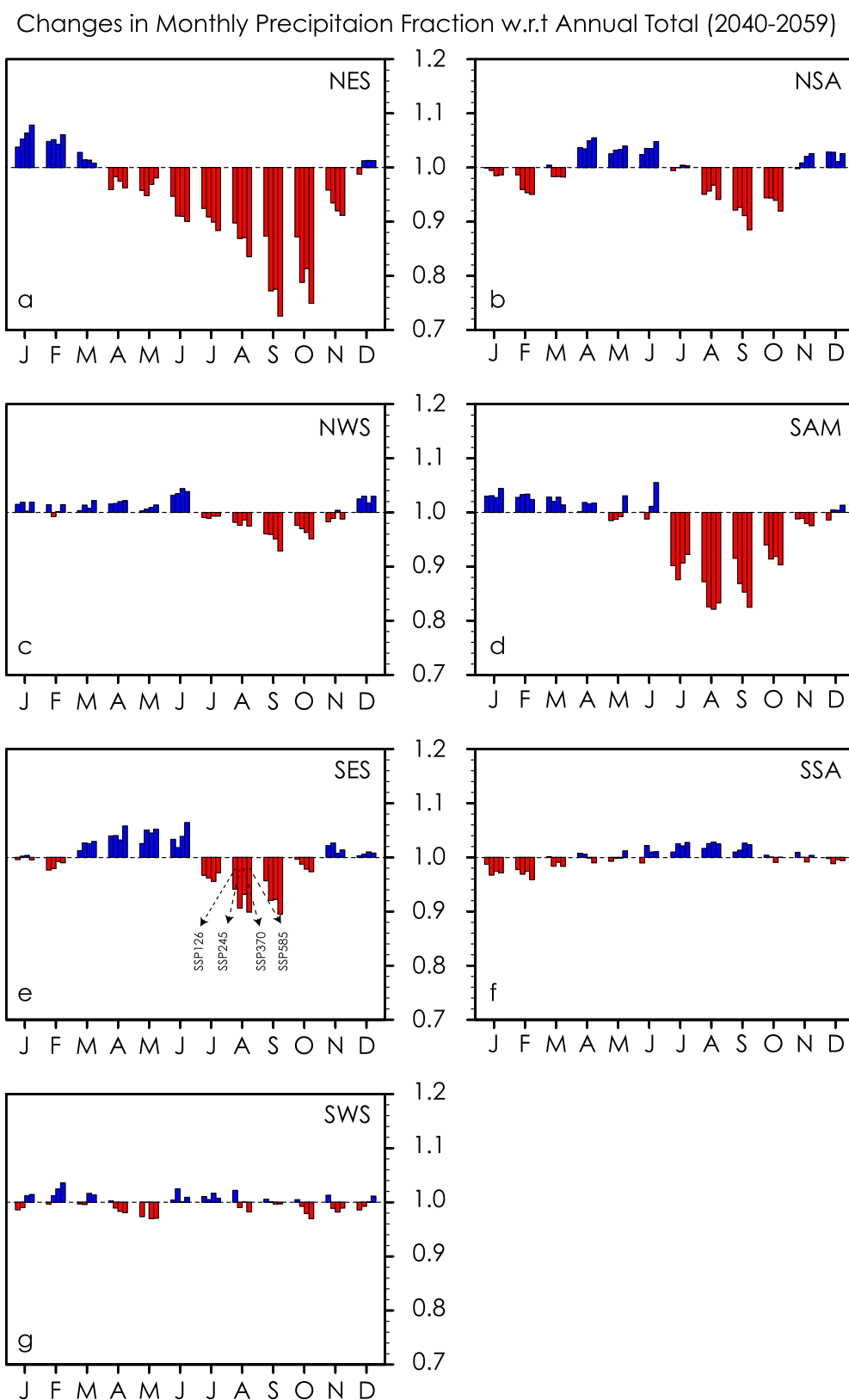
Fig. 13 Fractional changes in the monthly contributions to annual precipitation in the mid-century (2040–2059) future with respect to the reference period (1995–2014) under all four future scenarios. Blue (red) represents increase (decrease) in relative contribution. The results are based on the ensemble mean of GCMs

Fig. 14 Same as in Fig. 13 but for the late-century (2080–2099) future

Changes in Monthly Precipitaion Fraction w.r.t Annual Total (2080-2099)
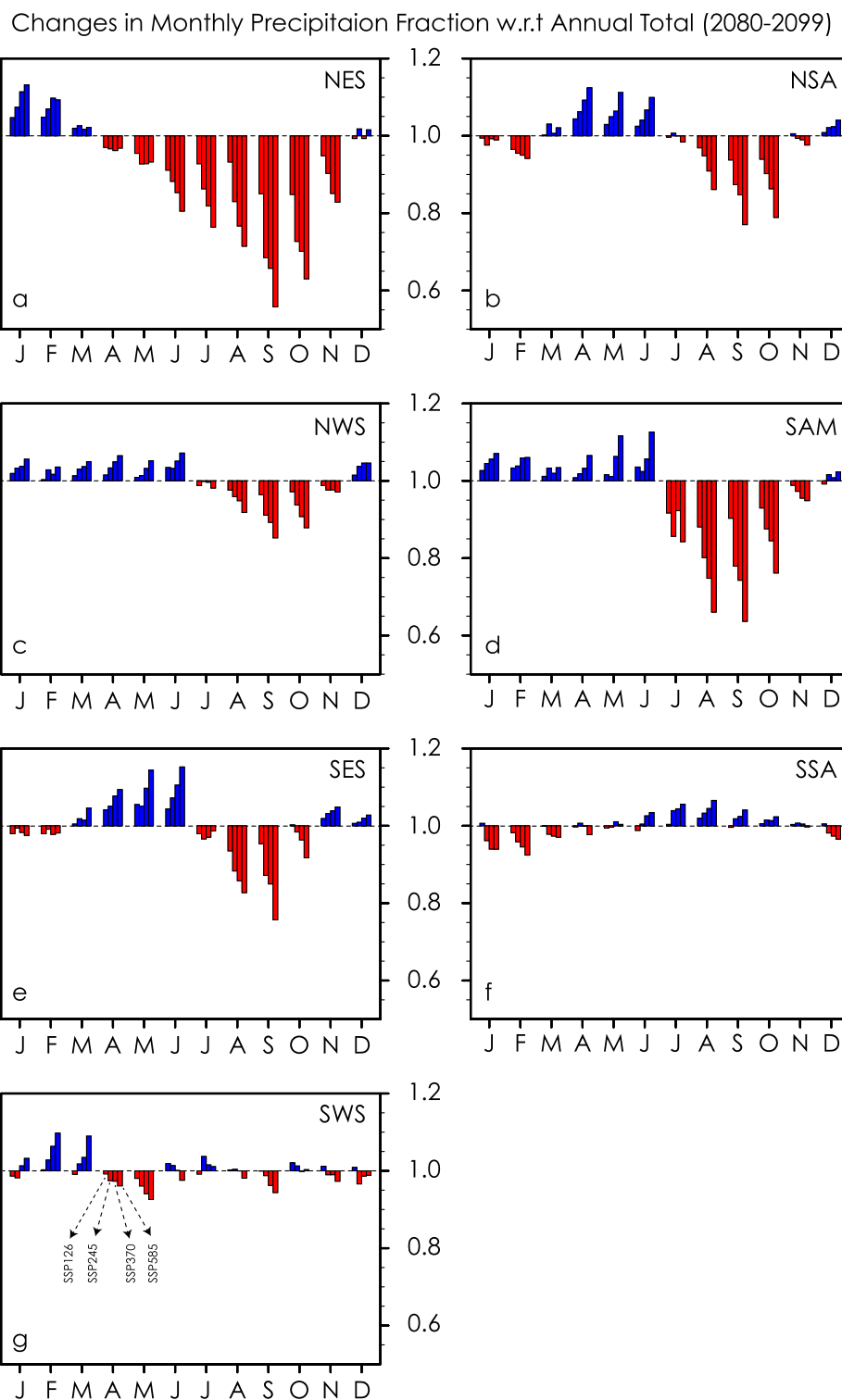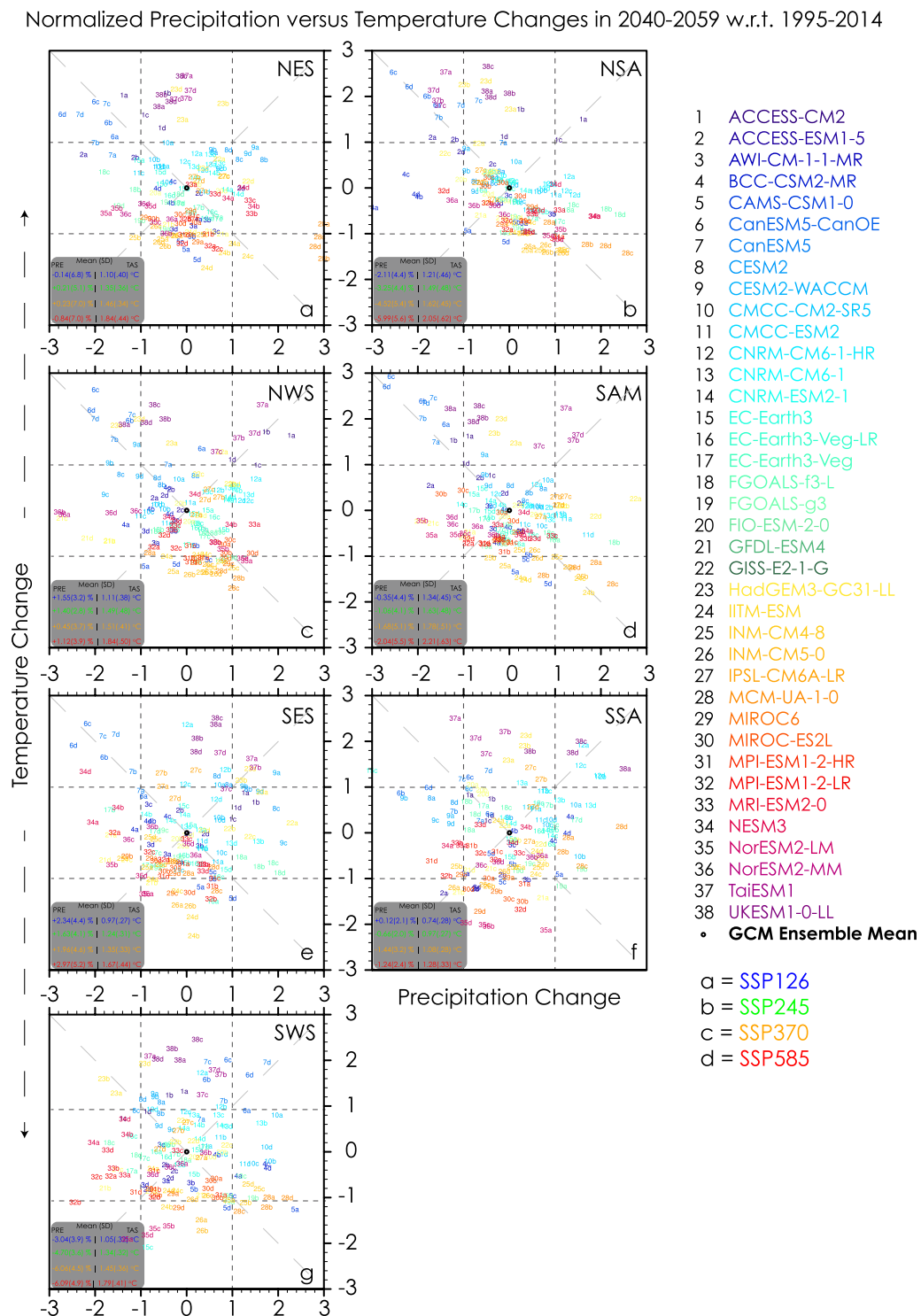
Fig. 15 Normalized precipitation change (%) versus temperature change (absolute) maps over seven sub-regions in the mid-century future (2040–2059) with respect to the reference period (1995–2014) under all four future scenarios. The GCM ensemble mean and 38 individual GCMs are averaged over each region and all 39 data points are normalized with respect to the mean and standard deviation across the sample (temperature/precipitation) space. The dotted blue lines represent 1 standard deviation (SD) along each axis. The numbers in the gray box represent ensemble mean and standard deviation across the ensemble for precipitation and temperature

Normalized Precipitation versus Temperature Changes in 2080-2099 w.r.t. 1995-2014
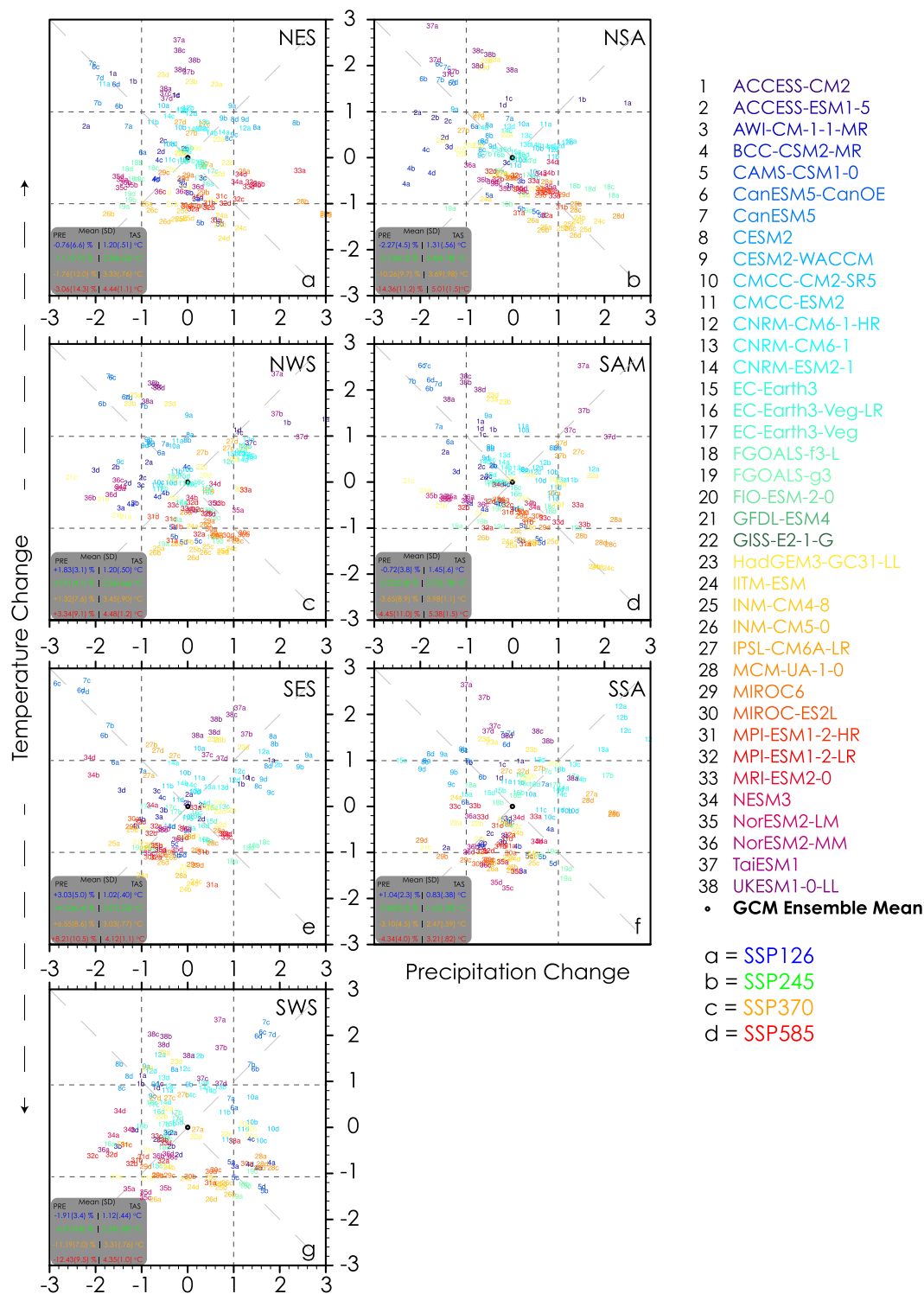
Fig. 16 Same as in Fig. 15 but for the late-century future (2080–2099)

precipitation characteristics can be avoided by following a lower emission trajectory (SSP126, SSP245; Figs. 8, 9, 11) as simulated changes remain within the reference period variability. However, our results indicate that a significantly different climate state in terms of temperature may be unavoidable in coming decades even after limiting the greenhouse gas emissions, as temperature increases become robust even when the lowest pathway is followed (SSP126; Fig. 10). The results also indicate a progressive increase in precipitation and temperature change with the strength of the future scenario, suggesting a relatively straightforward scaling in the projected change patterns that requires further detailed investigation in future studies. There is also an increase in the heterogeneity of precipitation distribution, as the relative contribution to annual total increases during the wettest part of the year—a finding consistent with earlier high-resolution modeling results (Ashfaq et al. 2020).

Apparently, there is no systematic linkage between model spread about the mean in the reference period and the magnitude of their simulated sub-regional climate change. The lack of a systematic relationship suggests that an outlier in the reference period is not necessarily an outlier in the simulated future responses and vice versa. However, further investigation is needed to fully understand such behavior. Nonetheless, the information regarding relative GCM distances from the mean in the reference period and their spread in the future climate projections is useful for regional downscaling or for climate impact studies where sub-selection of GCMs is necessary. Moreover, while this study only makes use of monthly precipitation and temperature, a progressive fat and heavy-tailed distribution of precipitation change, and a rightward shifted distribution of temperature change provide strong indications of increases in the intensity of the hydrological cycle with increased greenhouse gas emissions. Our results also highlight the limitations in the use of the Intergovernmental Panel on Climate Change updated climate reference sub-regions over areas where climate and landscape characteristics are highly heterogeneous (e.g., NWS).

The projected climatic changes have strong implications for the already stressed social-ecological landscape across South America. The substantial drying over the Amazon rainforest can have domino impacts on global energy, water and carbon balances. The imbalance in the intra-annual precipitation distribution could have serious consequences for sustainable hydropower generation and agriculture. The combination of projected monthly temperature and precipitation extremes can be lethal in the form of prolonged and frequent droughts, heatwaves and wildfires. The projected warming will likely accelerate glacier retreat, which would further deplete water resources for communities in the Andes as well as in their foothills. The impacts of projected climatic changes are complex and manifold and their quantification requires reliable regional climate information. We believe that the results presented in this study will be useful for informing such studies.

Declarations

References

Almazroui M, Islam MN, Saeed F et al (2021) Projected changes in temperature and precipitation over the United States, Central America, and the Caribbean in CMIP6 GCMs. Earth Syst Environ 5:1–24. https://doi.org/10.1007/s41748-021-00199-5

Alves LM, Chadwick R, Moise A et al (2020) Assessment of rainfall variability and future change in Brazil across multiple timescales. Int J Climatol. https://doi.org/10.1002/joc.6818

Arias PA, Garreaud R, Poveda G, Espinoza JC, Molina-Carpio J, Masiokas M, Viale M, Scaff L, van Oevelen PJ (2021a) Hydroclimate of the andes part II: hydroclimate variability and subcontinental patterns. Front Earth Sci 8:505467. https://doi.org/10.3389/feart.2020.505467

Arias PA, Ortega G, Villegas LD, Martínez JA (2021b) Colombian climatology in CMIP5/CMIP6 models: persistent biases and improvements. Revista Facultad De Ingeniería Universidad De Antioquia. https://doi.org/10.17533/udea.redin.20210525

Ashfaq M (2020) Topographic controls on the distribution of summer monsoon precipitation over South Asia. Earth Syst Environ 4:667–683. https://doi.org/10.1007/s41748-020-00196-0

Ashfaq M, Rastogi D, Mei R, Kao S-C, Gangrade S, Naz BS, Touma D (2016) High-resolution ensemble projections of near-term regional climate over the continental US. J Geophys Res-Atmos. https://doi.org/10.1002/2016JD025285

Ashfaq M, Cavazos T, Reboita MS et al (2020) Robust late twenty-first century shift in the regional monsoons in RegCM-CORDEX simulations. Clim Dyn. https://doi.org/10.1007/s00382-020-05306-2

Baez-Villanueva OM, Zambrano-Bigiarini M, Ribbe L, Nauditt A, Giraldo-Osorio JD, Thinh NX (2018) Temporal and spatial evaluation of satellite rainfall estimates over different regions in Latin-America. Atmos Res 213:34–50. https://doi.org/10.1016/j.atmosres.2018.05.011

Barkhordarian A, Saatchi SS, Behrangi A et al (2019) A recent systematic increase in vapor pressure deficit over tropical South America. Sci Rep 9:15331. https://doi.org/10.1038/s41598-019-51857-8

Barros VR, Boninsegna JA, Camilloni IA, Chidiak M, Magrín GO, Rusticucci M (2015) Climate change in Argentina: trends, projections, impacts and adaptation. Wiley Interdiscipy Rev Clim Change 6(2):151–169

Bellprat O, Lott FC, Gulizia C et al (2015) Unusual past dry and wet rainy seasons over Southern Africa and South America from a climate perspective. Weather Clim Extrem 9:36–46

Beck H, Zimmermann N, McVicar T et al (2018) Present and future Köppen–Geiger climate classification maps at 1-km resolution. Sci Data 5:180214. https://doi.org/10.1038/sdata.2018.214

Boisier JP, Ciais P, Ducharne A, Guimberteau M (2015) Projected strengthening of Amazonian dry season by constrained climate model simulations. Nat Clim Change 5(7):656–660

Bozkurt D, Rojas M, Boisier JP et al (2019) Dynamical downscaling over the complex terrain of southwest South America: present climate conditions and added value analysis. Clim Dyn 53:6745–6767. https://doi.org/10.1007/s00382-019-04959-y

Brando PM, Balch JK, Nepstad DC et al (2014) Abrupt increases in Amazonian tree mortality due to drought–fire interactions. Proc Natl Acad Sci 111(17):6347–6352

Brando PM, Paolucci L, Ummenhofer CC, Ordway EM, Hartmann H, Cattau ME, Rattis L, Medjibe V, Coe MT, Balch J (2019) Droughts, wildfires, and forest carbon cycling: a pantropical synthesis. Ann Rev Ear Planet Sci 47:555–581. https://doi.org/10.1146/annurev-earth-082517-010235

Carvalho LM (2020) Assessing precipitation trends in the Americas with historical data: a review. Wiley Interdiscip Rev Clim Change 11(2):e627. https://doi.org/10.1002/wcc.627

Chavez SP, Takahashi K (2017) Orographic rainfall hot spots in the Andes–Amazon transition according to the TRMM precipitation radar and in situ data. J Geophy Res: Atmos 122(11):5870–5882. https://doi.org/10.1002/2016JD026282

Chavez SP, Silva Y, Barros AP (2020) High-elevation monsoon precipitation processes in the Central Andes of Peru. J Geophys Res Atmos 125(24):e2020JD032947. https://doi.org/10.1029/2020JD032947

Chou SC, Lyra A, Mourão C et al (2014) Evaluation of the eta simulations nested in three global climate models. Am J Clim Chang 3:438–454. https://doi.org/10.4236/ajcc.2014.35039

Coelho CA, Cardoso DH, Firpo MA (2016) Precipitation diagnostics of an exceptionally dry event in São Paulo, Brazil. Theo Appl Climatol 125(3):769–784. https://doi.org/10.1007/s00704-015-1540-9

Condom T, Martínez R, Pabón JD, Costa F, Pineda L, Nieto JJ, López F, Villacis M (2020) Climatological and Hydrological Observations for the South American Andes: in situ stations, satellite, and reanalysis data sets. Front Earth Sci 8:92. https://doi.org/10.3389/feart.2020.00092

Cook BI, Mankin JS, Marvel K, Williams AP, Smerdon JE, Anchukaitis KJ (2020) Twenty-first century drought projections in the CMIP6 forcing scenarios. Earth's Future 8:e2019EF001461. https://doi.org/10.1029/2019EF001461

Cunha AP, Zeri M, Deusdará Leal K et al (2019) Extreme drought events over Brazil from 2011 to 2019. Atmos 10(11):642. https://doi.org/10.3390/atmos10110642

de Barros SD, Lee H, Loikith PC et al (2017) Can significant trends be detected in surface air temperature and precipitation over South America in recent decades? Int J Climatol 37(3):1483–1493

De Faria BL, Brando PM, Macedo MN et al (2017) Current and future patterns of fire-induced forest degradation in Amazonia. Environ Res Lett 12(9):095005

Debortoli NS, Sung CL, Hirota M (2020) Assessing farmers' vulnerability to extreme weather events in the Araranguá river watershed—southern Brazil. Vulnerability Studies in the Americas: Extrem Wea Clim Chang, p 125

Dereczynski C, Chou SC, Lyra A et al (2020) Downscaling of climate extremes over South America—part I: model evaluation in the reference climate. Wea Clim Extr 29:100273

Dias CG, Reboita MS (2021) Assessment of CMIP6 Simulations over Tropical South America. Braz J Phys Geogr (**accepted**)

Diaz LB, Saurral R, Vera C (2021) Assessment of South America summer rainfall climatology and trends in a set of global climate models large ensembles. Int J Climatol. https://doi.org/10.1002/joc.6643

Doss-Gollin J, Muñoz ÁG, Mason SJ, Pastén M (2018) Heavy rainfall in Paraguay during the 2015/16 austral summer: causes and subseasonal-to-seasonal predictive skill. J Clim 31(17):6669–6685. https://doi.org/10.1175/JCLI-D-17-0805.1

Drenkhan F, Guardamino L, Huggel C, Frey H (2018) Current and future glacier and lake assessment in the deglaciating Vilcanota–Urubamba basin, Peruvian Andes. Glob Plan Change 169:105–118. https://doi.org/10.1016/j.gloplacha.2018.07.005

Duffy PB, Brando P, Asner GA, Field CB (2015) Amazon extreme weather events. Proc Natl Acad Sci 112(43):13172–13177. https://doi.org/10.1073/pnas.1421010112

Durán-Quesada AM, Reboita M, Gimeno L (2012) Precipitation in tropical America and the associated sources of moisture: a short review. Hydro Sci J 57(4):612–624. https://doi.org/10.1080/02626667.2012.673723

Espinoza JC, Ronchail J, Marengo JA, Segura H (2019) Contrasting North-South changes in Amazon wet-day and dry-day frequency and related atmospheric features (1981–2017). Clim Dyn 52(9):5413–5430. https://doi.org/10.1007/s00382-018-4462-2

Espinoza JC, Garreaud R, Poveda G et al (2020) Hydroclimate of the Andes part I: main climate features. Front Earth Sci 8:64. https://doi.org/10.3389/feart.2020.00064

Falco M, Carril AF, Menéndez CG et al (2019) Assessment of CORDEX simulations over South America: added value on seasonal climatology and resolution considerations. Clim Dyn 52:4771–4786. https://doi.org/10.1007/s00382-018-4412-z

Feron S, Cordero RR, Damiani A et al (2019) Observations and projections of heat waves in South America. Sci Rep 9(1):8173. https://doi.org/10.1038/s41598-019-44614-4

Forbes C, Evans M, Hastings N, Peacock B (2011) Statistical distributions, 4th edn. Wiley, United States

Garreaud RD, Vuille M, Compagnucci R, Marengo J (2009) Present-day South American climate. Palaeogeograpr Palaeoclimatol, Palaeoecol 281:180–195. https://doi.org/10.1016/j.palaeo.2007.10.032

Giráldez L, Silva Y, Zubieta R, Sulca J (2020) Change of the rainfall seasonality over Central Peruvian Andes: onset, end, duration and its relationship with large-scale atmospheric circulation. Climate 8(2):23. https://doi.org/10.3390/cli8020023

Grimm AM, Dominguez F, Cavalcanti IFA et al. (2020) South and North American monsoons: characteristics, life cycle, variability, modelling and prediction. In: Chang CP, Ha KJ, Johnson RH, Kim D, Lau GNC, Wang B (eds) The multi-scale global monsoon system, World Scientific Series on Asia–Pacific Weather and Climate, Vol. 11, World Scientific Publishing Company, Singapore, 500 pp., Chapter 5, p 49–66. ISBN: 978-981-121-659-6

Gulizia C, Camilloni I (2015) Comparative analysis of the ability of a set of CMIP3 and CMIP5 global climate models to represent precipitation in South America. Int J Climatol 35(4):583–595. https://doi.org/10.1002/joc.4005

Hawkins E, Sutton RT (2009) The potential to narrow uncertainty in regional climate predictions. Bull Am Meteorol Soc 90:1095–1107. https://doi.org/10.1175/2009BAM-S2ensamblede607.1

Iturbide M, Gutiérrez JM, Alves LM et al (2020) An update of IPCC climate reference regions for subcontinental analysis of climate model data: definition and aggregated datasets. Earth Syst Sci Data. https://doi.org/10.5194/essd-2019-258

Kumar S, Moya-Álvarez AS, Castillo-Velarde CD et al (2020) Effect of low-level flow and Andes mountain on the tropical and mid-latitude precipitating cloud systems: GPM observations. Theor Appl Climatol 141:157–172. https://doi.org/10.1007/s00704-020-03155-x

Lemes MDCR, Reboita MS, Capucin BC (2020) Impactos das queimadas na Amazônia no tempo em São Paulo na tarde do dia 19 de agosto de 2019. Revista Brasileira De Geografia Física 13(3):983–993

Llopart M, Reboita MS, da Rocha RP (2020a) Assessment of multimodel climate projections of water resources over South America CORDEX domain. Clim Dyn 54(1):99–116. https://doi.org/10.1007/s00382-019-04990-z

Llopart M, Domingues LM, Torma C et al (2020b) Assessing changes in the atmospheric water budget as drivers for precipitation change over two CORDEX-CORE domains. Clim Dyn. https://doi.org/10.1007/s00382-020-05539-1

López-Moreno JI, Fontaneda S, Bazo J et al (2014) Recent glacier retreat and climate trends in Cordillera Huaytapallana, Peru. Glob Planet Chang 112:1–11. https://doi.org/10.1016/j.gloplacha.2013.10.010

Malmros JK, Mernild SH, Wilson R, Yde JC, Fensholt R (2016) Glacier area changes in the central Chilean and Argentinean Andes 1955–2013/14. J Glaciol 62(232):391–401. https://doi.org/10.1017/jog.2016.43

Marengo JA, Liebmann B, Grimm AM et al (2012) Recent developments on the South American monsoon system. Int J Climatol 32:1–21. https://doi.org/10.1002/joc.2254

Marengo JA, Souza CM Jr, Thonicke K et al (2018) Changes in climate and land use over the Amazon Region: current and future variability and trends. Front Earth Sci. https://doi.org/10.3389/feart.2018.00228

Marrafon VH, Reboita MS (2020) Características da precipitação na América do Sul reveladas através de índices climáticos. Revista Brasileira de Climatologia 26

Martins ES, Coelho CA, Haarsma R et al (2018) A multimethod attribution analysis of the prolonged northeast Brazil hydrometeorological drought (2012–16). Explaining extreme events of 2016 from a climate perspective. Spec Suppl Bull Am Meteorol Soc 99(1):S65–S69. https://doi.org/10.1175/BAMS-D-17-0102.1

Masiokas MH, Rabatel A, Rivera A, Ruiz L, Pitte P, Ceballos JL, Barcaza G, Soruco A, Bown F, Berthier E, Dussaillant I, MacDonell S (2020) A review of the current state and recent changes of the Andean cryosphere. Front Earth Sci 8:99. https://doi.org/10.3389/feart.2020.00099

Mejía JF, Yepes J, Henao JJ, Poveda G, Zuluaga MD, Raymond DJ, Fuchs-Stone Ž (2021) Towards a mechanistic understanding of precipitation over the far eastern tropical Pacific and western Colombia, one of the rainiest spots on Earth. J Geophys Res Atmos 126:e2020JD033415. https://doi.org/10.1029/2020JD033415

Montini TL, Jones C, Carvalho LM (2019) The South American low-level jet: a new climatology, variability, and changes. J Geophy Res Atmos 124(3):1200–1218. https://doi.org/10.1029/2018JD029634

Muñoz ÁG, Goddard L, Robertson AW et al (2015) Cross-time scale interactions and rainfall extreme events in southeastern South America for the austral summer. Part I: potential predictors. J Clim 28(19):7894–7913. https://doi.org/10.1175/JCLI-D-14-00693.1

Muñoz ÁG, Goddard L, Mason SJ, Robertson AW et al (2016) Cross-time scale interactions and rainfall extreme events in south-eastern south America for the austral summer. Part II: predictive skill. J Clim 29(16):5915–5934. https://doi.org/10.1175/JCLI-D-15-0699.1

Nielsen DM, Cataldi M, Belém AL, Albuquerque ALS (2016) Local indices for the South American monsoon system and its impacts on Southeast Brazilian precipitation patterns. Nat Hazards 83(2):909–928. https://doi.org/10.1007/s11069-016-2355-4

O'Neill BC et al (2016) The scenario model intercomparison project (ScenarioMIP) for CMIP6. Geosci Model Dev 9:3461–3482. https://doi.org/10.5194/gmd-9-3461-2016

Ortega G, Arias PA, Villegas JC, Marquet PA, Nobre P (2021) Present-day and future climate over Central and South America according to CMIP5/CMIP6 models. Int J Climatol. https://doi.org/10.1002/joc.7221

Ortiz-Jiménez MA (2018) Quantitative evaluation of the risk of Vibrio parahaemolyticus through consumption of raw oysters (Crassostrea corteziensis) in Tepic, Mexico, under the RCP2. 6 and RCP8. 5 climate scenarios at different time horizons. Food Res Int 111:111–119. https://doi.org/10.1016/j.foodres.2018.05.012

Pabón-Caicedo JD, Arias PA, Carril AF et al (2020) Observed and projected hydroclimate changes in the Andes. Front Earth Sci 8:61. https://doi.org/10.3389/feart.2020.00061

Paca VHDM, Espinoza-Dávalos GE, Moreira DM, Comair G (2020) Variability of trends in precipitation across the Amazon River basin determined from the CHIRPS precipitation product and from station records. Water 12(5):1244. https://doi.org/10.3390/w12051244

Palomino-Lemus R, Córdoba-Machado S, Gámiz-Fortis SR, Castro-Díez Y, Esteban-Parra MJ (2015) Summer precipitation projections over northwestern South America from CMIP5 models. Glob Planet Change. https://doi.org/10.1016/j.gloplacha.2015.05.004

Palomino-Lemus R, Córdoba-Machado S, Gámiz-Fortis SR, Castro-Díez Y, Esteban-Parra MJ (2017) Climate change projections of boreal summer precipitation over tropical America by using statistical downscaling from CMIP5 models. Environ Res Lett 12(12). https://iopscience.iop.org/article/https://doi.org/10.1088/1748-9326/aa9bf7/meta

Parsons LA (2020) Implications of CMIP6 projected drying trends for 21st century Amazonian drought risk. Earth's Future 8:e2020EF001608. https://doi.org/10.1029/2020EF001608

Petrie R, Denvil S, Ames S et al (2021) Coordinating an operational data distribution network for CMIP6 data. Geosci Mod Dev 14:629–644. https://doi.org/10.5194/gmd-14-629-2021

Pérez A, Gutiérrez D, Saldarriaga MS, Sanders CJ (2017) Hydrological controls on the biogeochemical dynamics in a Peruvian mangrove forest. Hydrobiologia 803:69–86. https://doi.org/10.1007/s10750-017-3118-2

Pendergrass AG, Knutti R, Lehner F et al (2017) Precipitation variability increases in a warmer climate. Sci Rep 7:17966. https://doi.org/10.1038/s41598-017-17966-y

Phillips OL, Brienen RJW, the RAINFOR collaboration (2017) Carbon uptake by mature Amazon forests has mitigated Amazon nations' carbon emissions. Carbon Balance Manag 12:1. https://doi.org/10.1186/s13021-016-0069-2

Poveda G, Mesa O (2000) On the existence of Lloró (the rainiest locality on Earth): enhanced ocean-land-atmosphere interaction by a low-level jet. Geophys Res Lett. https://doi.org/10.1029/1999GL006091

Rabatel A, Francou B, Soruco A et al (2013) Current state of glaciers in the tropical Andes: a multi-century perspective on glacier evolution and climate change. Cryosphere 7:81–102. https://doi.org/10.5194/tc-7-81-2013

Reboita MS, Gan MA, Rocha RPD, Ambrizzi T (2010) Precipitation regimes in South America: a bibliography review. Revista Brasileira De Meteorologia 25(2):185–204. https://doi.org/10.1590/S0102-77862010000200004

Reboita MS, da Rocha RP, Dias CG, Ynoue RY (2014) Climate projections for South America: RegCM3 driven by HadCM3 and ECHAM5. Adv Meteorol. https://doi.org/10.1155/2014/376738

Reboita MS, Rodrigues M, Armando R, Freitas C, Martins D, Miller G (2016) The causes of semi-aridity in the Northeast "Sertão". Braz J Climatol. https://doi.org/10.5380/abclima.v19i0.42091

Riahi K, Rao S, Krey V, Cho C, Chirkov V, Fischer G, Kindermann G, Nakicenovic N, Rafaj P (2011) RCP 8.5—a scenario of comparatively high greenhouse gas emissions. Clim Change 109(1):33–57. https://doi.org/10.1007/s10584-011-0149-y

Riahi K, Van Vuuren DP, Kriegler E, Edmonds J, O'Neill BC, Fujimori S et al (2017) The shared socioeconomic pathways and their energy, land use, and greenhouse gas emissions implications: an overview. Glob Environ Changw 42:153–168. https://doi.org/10.1016/j.gloenvcha.2016.05.009

Ritter B, Wennrich V, Medialdea A et al (2019) Climatic fluctuations in the hyperarid core of the Atacama Desert during the past 215 ka. Sci Rep 9(1):1–13. https://doi.org/10.1038/s41598-019-41743-8

Rivera JA, Arnould G (2020) Evaluation of the ability of CMIP6 models to simulate precipitation over Southwestern South America: climatic features and long-term trends (1901–2014). Atmos Res 241:104953. https://doi.org/10.1016/j.atmosres.2020.104953

Salviano MF, Groppo JD, Pellegrino GQ (2016) Análise de tendências em dados de precipitação e temperatura no Brasil. Revista Brasileira De Meteorologia 31(1):64–73. https://doi.org/10.1590/0102-778620150003

Sánchez E, Solman S, Remedio ARC et al (2015) Regional climate modelling in CLARIS-LPB: a concerted approach towards twentyfirst century projections of regional temperature and precipitation over South America. Clim Dyn 45:2193–2212. https://doi.org/10.1007/s00382-014-2466-0

Schauwecker S, Rohrer M, Acuña D et al (2014) Climate trends and glacier retreat in the Cordillera Blanca, Peru, revisited. Glob Planet Change 119:85–97. https://doi.org/10.1016/j.gloplacha.2014.05.005

Schumacher V, Justino F, Fernández A, Meseguer-Ruiz O, Sarricolea P, Comin A, Peroni Venancio L, Althoff D (2020) Comparison between observations and gridded data sets over complex terrain in the Chilean Andes: precipitation and temperature. Int J Climatol 40(12):5266–5288. https://doi.org/10.1002/joc.6518

Schween JH, Hoffmeister D, Löhnert U (2020) Filling the observational gap in the Atacama Desert with a new network of climate stations. Glob Planet Change 184:103034. https://doi.org/10.1016/j.gloplacha.2019.103034

Sena TACT, Magnusdottir G (2020) Projected End-of-Century Changes in the South American Monsoon in the CESM Large Ensemble. J Clim 33(18): 7859–7874. https://journals.ametsoc.org/view/journals/clim/33/18/jcliD190645.xm

Sierra JP, Arias PA, Vieira SC (2015) Precipitation over northern South America and its seasonal variability as simulated by the CMIP5 models. Adv Meteorol. https://doi.org/10.1155/2015/634720

Silva CV, Aragão LE, Barlow J, Espirito-Santo F, Young PJ, Anderson LO, Xaud HA (2018) Drought-induced Amazonian wildfires instigate a decadal-scale disruption of forest carbon dynamics. Philo Trans R Soc b: Biol Sci 373(1760):20180043. https://doi.org/10.1098/rstb.2018.0043

Silva Dias MAF, Carvalho LMV (2017) The South American Monsoon System. World Sci Ser Asia-Pac Weather Clim. https://doi.org/10.1142/9789813200913_0003

Somers LD, McKenzie JM, Mark BG, Lagos P, Ng GHC, Wickert AD, Silva Y (2019) Groundwater buffers decreasing glacier melt in an Andean watershed—but not forever. Geophy Res Lett 46(22):13016–13026. https://doi.org/10.1029/2019GL084730

Spinoni J, Vogt J, Naumann G, Carrao H, Barbosa P (2015) Towards identifying areas at climatological risk of desertification using the Köppen–Geiger classification and FAO aridity index. Int J Climatol 35:2210–2222. https://doi.org/10.1002/joc.4124

Thaler V, Loikith PC, Mechoso CR, Pampuch LA (2021) A multivariate assessment of climate change projections over South America using the fifth phase of the Coupled Model Intercomparison Project. Int J Climatol. https://doi.org/10.1002/joc.7072

Tian B, Dong X (2020) The double-ITCZ bias in CMIP3, CMIP5, and CMIP6 models based on annual mean precipitation. Geophys Res Lett. https://doi.org/10.1029/2020GL087232

van Vuuren DP, Edmonds J, Kainuma M et al (2011) The representative concentration pathways: an overview. Clim Change 109(1):5–31. https://doi.org/10.1007/s10584-011-0148-z

Veettil BK, Kamp U (2019) Global disappearance of tropical mountain glaciers: observations, causes, and challenges. Geosciences 9(5):196. https://doi.org/10.3390/geosciences9050196

Vera C, Baez J, Douglas M, Emmanuel CB, Marengo J et al (2006) The South American low-level jet experiment. Bull Am Meteorol Soc 87(1):63–78. https://journals.ametsoc.org/view/journals/bams/87/1/bams-87-1-63.xml

Vieira RMDSP, Tomasella J, Barbosa AA et al (2021) Desertification risk assessment in Northeast Brazil: current trends and future scenarios. Wiley. https://doi.org/10.1002/ldr.3681

Viganó HHDG, Souza CCD, Reis Neto JF, Cristaldo MF, Jesus LD (2018) Prediction and modeling of forest fires in the Pantanal. Revista Brasileira De Meteorologia 33(2):306–316. https://doi.org/10.1590/0102-7786332012

Vuille M, Carey M, Huggel C, Buytaert W, Rabatel A, Jacobsen D, Sicart JE (2018) Rapid decline of snow and ice in the tropical Andes—impacts, uncertainties and challenges ahead. Earth-Sci Rev 176:195–213. https://doi.org/10.1016/j.earscirev.2017.09.019

Yarleque C, Vuille M, Hardy DR et al (2018) Projections of the future disappearance of the Quelccaya Ice Cap in the Central Andes. Sci Rep 8:15564. https://doi.org/10.1038/s41598-018-33698-z

Yin L, Fu R, Shevliakova E et al (2013) How well can CMIP5 simulate precipitation and its controlling processes over tropical South

America? Clim Dyn 41:3127–3143. https://doi.org/10.1007/s00382-012-1582-y

Zazulie N, Rusticucci M, Raga GB (2017) Regional climate of the subtropical central Andes using high-resolution CMIP5 models—part I: past performance (1980–2005). Clim Dyn 49:3937–3957. https://doi.org/10.1007/s00382-017-3560-x

Zazulie N, Rusticucci M, Raga GB (2018) Regional climate of the Subtropical Central Andes using high-resolution CMIP5 models. Part II: future projections for the twenty-first century. Clim Dyn 51(7):2913–2925. https://doi.org/10.1007/s00382-017-4056-4

Zelinka MD, Myers TA, McCoy DT, Po-Chedley S, Caldwell PM, Ceppi P, Klein SA, Taylor KE (2020) Causes of higher climate sensitivity in CMIP6 models. Geophy Res Lett 47(1):e2019GL085782. https://doi.org/10.1029/2019GL085782

Zhang K, de Castanho ADA, Galbraith DR (2015) The fate of Amazonian ecosystems over the coming century arising from changes in climate, atmospheric CO_2, and land use. Glob Change Biol 21(7):2569–2587. https://doi.org/10.1111/gcb.12903

Zubieta R, Saavedra M, Espinoza JC et al (2019) Assessing precipitation concentration in the Amazon basin from different satellite-based data sets. Int J Climatol 39:3171–3187. https://doi.org/10.1002/joc.6009

Zubieta R, Molina-Carpio J, Laqui W, Sulca J, Ilbay M (2021) Comparative analysis of climate change impacts on meteorological, hydrological, and agricultural droughts in the lake Titicaca basin. Water 13(2):175. https://doi.org/10.3390/w13020175

Authors and Affiliations

Mansour Almazroui[1,2] · Moetasim Ashfaq[3] · M. Nazrul Islam[1] · Irfan Ur Rashid[4] · Shahzad Kamil[4] · Muhammad Adnan Abid[5] · Enda O'Brien[6] · Muhammad Ismail[1] · Michelle Simões Reboita[7] · Anna A. Sörensson[8,9,10] · Paola A. Arias[11] · Lincoln Muniz Alves[12] · Michael K. Tippett[13] · Sajjad Saeed[5,14] · Rein Haarsma[15] · Francisco J. Doblas-Reyes[16,17] · Fahad Saeed[18] · Fred Kucharski[5] · Imran Nadeem[19] · Yamina Silva-Vidal[20] · Juan A. Rivera[21,22] · Muhammad Azhar Ehsan[23] · Daniel Martínez-Castro[24] · Ángel G. Muñoz[23] · Md. Arfan Ali[25] · Erika Coppola[5] · Mouhamadou Bamba Sylla[26]

1   Centre of Excellence for Climate Change Research/Department of Meteorology, King Abdulaziz University, Jeddah 21589, Saudi Arabia

2   Climatic Research Unit, School of Environmental Sciences, University of East Anglia, Norwich, UK

3   Computational Sciences and Engineering Division, Oak Ridge National Laboratory, Oak Ridge, TN, USA

4   Climate Change Impact and Integration Cell (CIIC), Pakistan Meteorological Department, Islamabad, Pakistan

5   Earth System Physics Section, The Abdus Salam International Centre for Theoretical Physics (ICTP), Trieste, Italy

6   Irish Centre for High-End Computing, Galway, Ireland

7   Federal University of Itajubá, Itajubá, Brazil

8   Facultad de Ciencias Exactas y Naturales, Departamento de Ciencias de la Atmósfera y los Océanos, Universidad de Buenos Aires, Buenos Aires, Argentina

9   Centro de Investigaciones del Mar y la Atmósfera (CIMA), CONICET, Universidad de Buenos Aires, Buenos Aires, Argentina

10 CNRS, IRD, CONICET, UBA, Instituto Franco-Argentino Para el Estudio del Clima y Sus Impactos (IRL 3351 IFAECI), Buenos Aires, Argentina

11 Grupo de Ingeniería y Gestión Ambiental (GIGA), Escuela Ambiental, Facultad de Ingeniería, Universidad de Antioquia, Medellin, Colombia

12 Instituto Nacional de Pesquisas Espaciais (INPE), São José de Campos, São Paulo, Brazil

13 Department of Applied Physics and Applied Mathematics, Columbia University, New York, USA

14 Department of Earth and Environmental Sciences, University of Leuven (KU Leuven), Leuven, Belgium

15 Royal Netherlands Meteorological Institute (KNMI), De Bilt, Netherlands

16 Institució Catalana de Recerca I Estudis Avançats (ICREA), Barcelona, Spain

17 Barcelona Supercomputing Center (BSC), Barcelona, Spain

18 Climate Analytics, Berlin, Germany

19 Institute of Meteorology and Climatology, University of Natural Resources and Life Sciences, Vienna, Austria

20 Instituto Geofísico del Perú, Lima, Perú

21 Instituto Argentino de Nivología, Glaciología y Ciencias Ambientales (IANIGLA), CCT CONICET Mendoza, Mendoza, Argentina

22 Universidad Juan Agustín Maza, Mendoza, Argentina

23 International Research Institute for Climate and Society (IRI), The Earth Institute At Columbia University, Palisades, NY, USA

24 Instituto Nacional de Investigaciones en Glaciares y Ecosistemas de Montaña, Huaraz, Ancash, Perú

25 Lab of Environmental Remote Sensing, School of Marine Sciences (SMS), Nanjing University of Information Science and Technology (NUIST), Nanjing 210044, China

26 African Institute for Mathematical Sciences, Kigali, Rwanda